Wear and friction performance evaluation of nickel based nanocomposite coatings under refrigerant lubrication

Muhammad Usman Bhutta [a,b], Zulfiqar Ahmad Khan [a,*]

[a] Bournemouth University, Department of Design & Engineering, NanoCorr, Energy & Modelling (NCEM) Research Group, Dorset BH12 5BB, United Kingdom
[b] School of Mechanical & Manufacturing Engineering (SMME), National University of Sciences & Technology (NUST), Campus H-12, Islamabad, Pakistan

ARTICLE INFO

ABSTRACT

Environmental concerns related to global warming has enforced the introduction of newly artificially formulated refrigerants. HFE-7000 is a replacement solution for the existing harmful refrigerants and thermo-fluids having a broad range of application areas including usage in green energy, low carbon technologies, in aerospace and automotive industries. In this study five different types of coatings namely, Ni–ZrO$_2$, Ni–Al$_2$O$_3$, Ni–SiC, Ni-Graphene and Nickel-only have been used to study the wear and friction performance of these coatings in systems based on HFE-7000 refrigerant. Extensive experimentation has been performed on these coated contacts using a modified pressurised lubricity tester by changing the refrigerant temperature and the applied normal load in an attempt to enhance the tribological performance of interacting machine parts employing HFE-7000. EDS analysis performed on all the sample pairs within the contact region revealed the presence of fluorine and oxygen based tribo-films. These oxygenated and fluorinated tribo-films help prevent metal-to-metal contact leading to a drop in friction and wear. All coatings presented an improvement in the micro-hardness and in hardness to elastic modulus ratio compared to uncoated steel. The results of friction and wear of coated samples were compared to uncoated steel as well. The results show an improvement in wear and friction at most of the operating conditions by applying Nickel based coatings on a steel substrate in the presence of HFE-7000. Friction and wear performance of Nickel based coatings does drop for some of the coatings at particular testing conditions which leads to conclude that a careful selection of the coatings has to be made depending on the operating refrigerant temperature and load. The results of this study provide a guideline and will be extremely useful in selecting the type of coating based on the application area.

1. Introduction

Over the past century refrigerants have slowly progressed from the first generation to their fourth generation [1]. The gradual progression and development of refrigerants is linked to their flammability, toxicity and environmental impact. Toxicity and flammability of the first generation of refrigerants which were naturally occurring led to the search for replacement refrigerants in the 1920s [2]. Research for non-flammable and non-toxic refrigerants brought forward the first family of artificially formulated refrigerants; CFCs (Chlorofluorocarbons) and HCFCs (Hydrochlorofluorocarbons). The destruction of the ozone layer by these refrigerants enforced a ban on CFCs and HCFCs through the Montreal Protocol on Substances that Deplete the Ozone layers in 1987 [3]. HFCs (Hydrofluorocarbons) were introduced as response to the ban on CFCs and HCFCs. In contrast to CFCs and HCFCs,

HFCs displayed poorer friction, wear and overall tribological performance [2]. The inferior friction, wear and tribological performance of HFCs is due to their inability to chemically react with the rubbing surfaces to produce protective surface tribo-films at typical compressor operating conditions [2]. In contrast CFCs and HCFCs reacted with the mating metal surfaces forming protective surface tribo-films which gave CFCs and HCFCs excellent tribological properties [2]. HFCs were later identified amongst the primary contributors to global warming and as per the 1997 Kyoto Protocol to the United Nations Framework Convention on Climate Change [4], these refrigerants are now in the process of being phased out. Naturally occurring compounds with zero Ozone Depletion Potential (ODP) and very low Global Warming Potential (GWP) have become of particular interest as well since the Kyoto Protocol in search for suitable replacement refrigerants.

Non-toxic, non-flammable Carbon dioxide which has a Global

Warming Potential value of one and an Ozone Depletion Potential value of zero has been studied for its tribological performance [5–10] as a possible replacement refrigerant. Operating pressures when using CO_2 however are extremely high compared to the traditional refrigerants which requires special equipment design for its viable commercialization [2]. Another family of environmental family refrigerants are Hydrocarbons (HCs) which have zero ODP and low GWP values have also been studied for their friction, wear, fatigue and overall power consumption [11–16]. HCs are used in domestic and commercial applications but are inheritably highly flammable which restricts their application areas.

As a result to the legislations on environmental impact and the toxicity/flammability issues of naturally occurring compounds the fourth generation of artificially formulated refrigerants which not only have zero ODP but also have lower GWP have been introduced [1,2].

Hydrofluoroethers (HFEs) are amongst the family of the fourth generation of future refrigerants having high commercialization potential and applications. HFE-7000 is a non-flammable, non-corrosive refrigerant having zero ODP, low GWP, good materials compatibility, excellent dielectric properties and good thermal stability [17]. Its applications include usage in fuel cells, in electronic cooling units, in medical laboratories, in chemical reactors, in freeze dryers, in dry etchers, in high voltage transformers, in auto-cascaded refrigeration systems, etc. [17]. HFE-7000 has a boiling point much higher than HFC-134a and is not considered a direct 'drop-in' solution and replacement of HFC-134a in compressors [2]. HFE-7000 has a broader range of fields where it can be utilized. It has been successfully used in renewable energy systems and low carbon technologies [18,19], in solar organic Rankine cycle [20], in Electrohydrodynamics applications [21], as a jet impinging dialectic coolant [22], etc. Different physical and chemical properties of Hydrofluoroether-7000 have been listed in Table 1. Various different properties of HFC-134a, which was a highly used Hydrofluorocarbon have also been listed in Table 1. Both HFE-7000 and HFC-134a have an ODP value of zero but the GWP value of HFE-7000 is about one third to that of HFC-134a. HFE-7000 has kinematic viscosity of 0.32 cSt at 20 °C, 0.29 cSt at 30 °C and 0.27 cSt at 40 °C [17].

This research has been conducted to assess the wear and friction behaviour of interacting parts at relatively low loads subject to nanocomposite coatings under HFE-7000 lubrication. This study is a continuation of our previous pilot study [24] which evaluated the possibility to enhance wear performance of rubbing parts by using Ni–Al_2O_3 nanocomposite coatings subject to HFE-7000 lubrication. The study showed a very significant enhancement in wear at low as well as high loads, but not at intermediate loads. In the current study five different types of coatings namely, Ni–ZrO_2, Ni–Al_2O_3, Ni–SiC, Ni-Graphene (Ni-GPL) and Nickel-only have been used with increased testing conditions. Nanostructured layout and design achieved through the electrodeposition of nano sized particles into the Nickel matrix has been proved to enhance friction, wear, corrosion and overall mechanical

Table 1
Different properties of HFE-7000 and HFC-134a [17,23,24].

Refrigerant	HFE-7000	HFC-134a
Structure	$C_3F_7OCH_3$	Ch_2FCF_3
Molecular Weight (g/mol)	200	102
Freezing Point (°C)	−122.5	−103.3
Boiling Point @ 1 atm (°C)	34	−26
Critical Temperature (°C)	165	101
Liquid Density (kg/m^3)	1400	1206
Critical Pressure (MPa)	2.48	4.06
Flash Point (°C)	None	250
Appearance	Clear, colourless	Colourless gas
Flammability	Non-flammable	Non-flammable
Ozone Depletion Potential (ODP)	Zero	Zero
Global Warming Potential (GWP)	530[a]	1430[a]

[a] GWP 100-year integrated time horizon (ITH). IPCC 2013 [25]

performance of interacting parts under a range of testing conditions [26–35].

A ball-on-flat disc contact geometry has been employed in this research by using a modified tribo-meter with HFE-7000 under saturated liquid state with fully lubricated conditions. All coatings were developed on a steel substrate through the pulse coating technique.

2. Materials and methods

A modified Phoenix Tribology TE-57/77 reciprocating tribo-meter as described in Ref. [24,36,37] was used in this study. The equipment is fully capable of testing the future generation of environmentally friendly refrigerates [24,36]. The apparatus provides the flexibility to vary the testing conditions by varying the operating temperature, by changing the applied normal load, by altering the reciprocating frequency and by controlling the chamber pressure. Details with description of the modified test rig are provided in Ref. [36].

AISI 52100 steel balls were used as the ball sample against normally loaded reciprocating nano coated flat samples. Each flat sample was coated on EN1A (230M07) steel. The flat sample is housed in the specimen cup which is then fastened on the reciprocating rod. The ball sample is fixed in the ball holder by grub screws which is then screwed to the horizontal shat. After the samples have been installed the test chamber is sealed after which it is vacuumed in order to reduce the effects of atmospheric air and ambient oxygen. Refrigerant is then introduced in to the vacuumed test chamber and fully lubricated conditions are established. The reciprocating frequency and refrigerant temperature are controlled through PID control. Chamber pressure is monitored and recorded through a pressure gauge and pressure transducer. The heater block is positioned at the very bottom of the chamber. A wire-type thermocouple is located directly inside the specimen and refrigerant cup which is used to monitor the refrigerant temperature. Data from all the transducers is continuously recorded, monitored and controlled using a purpose built software COMPEND.

2.1. Sample preparation

Flat circular samples having a diameter of 30 mm were machined into 2.75 mm thickness. Each flat specimen was then mechanically grinded followed by surface polishing to obtain an average surface roughness (R_a) of 0.05 μm. After the grinding and polishing process an ultrasonic bath was used to ultrasonically condition each test sample for 5 min with acetone, after which a specimen drier was used to dry each sample with warm air. The mechanical grinding and polishing process followed by the ultrasonic surface conditioning of each flat sample with acetone ensured the removal of any oxides or undesired surface films that might be present.

Coatings of ~10 μm thickness were deposited on the flat circular steel specimens through pulse electrodeposition. Five different electrolytic base solutions were prepared by using H_3BO_3, $NiSO_4\cdot6H_2O$ and $NiCl_2\cdot6H_2O$. Each base solution contained 31 g/L of H_3BO_3, 265 g/L of $NiSO_4\cdot6H_2O$ and 48 g/L of $NiCl_2\cdot6H_2O$. To develop Ni–Al_2O_3 nanocomposite coatings the first base solution was added with 20 g/L Al_2O_3 nanoparticles with average particle size of less than 50 nm. The second base solution was added with 20 g/L ZrO_2 nanoparticles having particle size between 20 and 30 nm for the development of Ni–ZrO_2 nanocomposite coatings. To deposit Ni–SiC nano coatings the third base solution was added with 20 g/L SiC nanoparticles having particle size between 50 and 60 nm. For the deposition of Ni-Graphene (Ni-GPL) nanocomposite coatings the fourth base solution was added with 0.1 g/L Graphene nanoparticles having particle size of 6–8 nm. Nano particles were not added in the fifth base solution as this solution was used in the preparation of pure Nickel coatings. Each solution was stirred magnetically for 24 h after which the nanoparticles containing solutions were ultrasonically agitated for 4 additional hours. This process confirmed proper dispersion and suspension of particles inside the solution. To start

the coating process each solution was heated to 40 °C after which a solution is ready for the deposition process. Grinded, polished and ultrasonically treated flat steel circular specimen was suspended in the prepared solution along with a pure Nickel sheet. The steel sample acted as the cathode and Nickel sheet was used as anode. For the deposition of nanocomposite coatings the solutions were ultrasonically agitated, magnetically stirred constantly and maintained at 40 °C during the entire deposition process. Pure Nickel coatings were prepared through the same process expect that Nickel-only solutions were not ultrasonically agitated. The duty cycle for pulse coating was fixed at 20% with pulse OFF-ON time of (80 ms–20 ms) with the current density being maintained at (3 A/dm^2). All the pulse parameters were maintained at a constant level throughout the coating process and deposition procedure was stopped after 1 h.

Microstructures of the developed coatings were studied using a Scanning Electron Microscope (SEM). Energy Dispersive X-ray Spectroscopic (EDS) Analysis were performed on each coating at several different regions on the surface. High magnification images and EDS results of all the coatings are shown in Fig. 1. EDS results clearly show the presence of Nickel on the top surface of each of the prepared coatings along with the presence of respective Nano particles embedded in the Nickel matrix. The microstructure and EDS results of these coatings is in accordance with the results reported by various researchers [32–34,38, 39]. These results show that coatings have been successfully prepared. The high magnification micrographs reveal pores on the top surface of all the coatings. These pores are randomly distributed on the surface of all the coatings and are better highlighted by applying false colour to the grayscale micrographs. These false coloured images of each coatings are also shown in Fig. 1. These pores are an inherent property of Nickel based nanocomposite coatings [24,32–34].

Grain size measurement was performed on all the prepared coatings pre-experimentation using optical microscopy. The results of the grain size measurement have been presented in Fig. 2. The grain size measurement results show Ni–SiC and Ni–ZrO$_2$ to have the highest results of maximum average grain size values flowed by Ni–Al$_2$O$_3$ and Ni-Only coatings, Ni-Graphene displayed the lowest results of the maximum average grain size values.

Ni-GPL coatings have been known to have refined grains, Ni–SiC and Ni–ZrO$_2$ have been reported to have large grains while Ni–Al$_2$O$_3$ have been observed to have larger grain size than Ni-GPL but smaller than Ni–SiC and Ni–ZrO$_2$ [34]. A cause of higher grain size of Ni–ZrO$_2$ and Ni–SiC is due to particle agglomeration [32], agglomerated particles are also present on Ni-GPL which gives rise to higher surface roughness values. Ni-GPL coatings deposited through electrodeposition on a steel substrate have been reported to develop bulges morphology and agglomeration effect which depends on the Watts bath temperature [40]. Increasing the temperature of the bath increases the surface roughness of the prepared coatings while a Watts bath temperature of 45 °C has been reported to produce minimum grain size and best hardness results [40]. The pulse electrodeposition of Ni-GPL produced coatings having maximum surface roughness values compared to all the other coatings.

A Nano indentation setup was used to measure the micro-hardness, the elastic modulus and to perform scratch tests on each of the prepared coatings. Depth controlled indentations were performed by keeping the depth of penetration of the indenter to 1/10 of the thickness of the coatings to mitigate the effects on the substrate on the measured data. The average surface roughness of all the coatings was measured through ZYGO (a white light interferometer). The results of the measured micro hardness, elastic modulus and average surface roughness have been presented in Table 2. Ni-GPL, Ni–Al$_2$O$_3$ and Ni–SiC nanocomposite coatings demonstrated the maximum nano-hardness values followed by Ni-ZO$_2$. Compared to the uncoated steel sample, an improvement in surface hardness was also shown by Nickel-only coatings. Micro-hardness improved for all the coated samples. Finer surface morphology of Ni–Al$_2$O$_3$ resulted in Ni–Al$_2$O$_3$ having the least values for

average surface roughness followed by pure Nickel, higher grain size and particle agglomeration cause higher surface roughness values for Ni–ZrO$_2$ and Ni–SiC [32,34]. The Pulse deposited Ni-GPL showed the maximum surface roughness values in contrast to all the prepared samples. The high average surface values of Ni-GPL is because of the presence of embedded graphene nanoparticles on the very top of the coated surface which gives Ni-GPL a rough surface finish and a blackish grey appearance. Ni-GPL are known to have coarser surface and higher surface roughness values at higher deposition temperatures [40].

Scratch tests were performed on all the coatings. The results of the scratch test have been shown in Fig. 3. The loading conditions were kept constant for all the scratch tests. Multi-pass Wear Tests were conducted with a scanning velocity of 20 μm/s with 4 passes and 2 scratches per topography. Scratch load of 150 mN was applied as following the loading shown in Fig. 3 (f) using spherical indenter of 5 μm. The multi-pass wear test results of the scratch test indicate Ni-GPL to have very good wear resistance, the spikes in the data are due to the high surface roughness value of Ni-GPL coating and due to the removal of the loosely embedded graphene nano particles from the top surface of the coating by applying the load during scratch test. Nickel only, Ni–Al$_2$O$_3$ and Ni-ZO$_2$ exhibited an increase in wear scratch depth on the second pass; maximum wear depth was noted for Nickel-only coatings. Ni–SiC coatings also showed good resistance to wear. The thickness of all the coatings was in the range of 8–10 μm and none of the scratches was able to penetrate the entire depth of a coating. In fact the penetration depth was less the 50% of the thickness of any given coating.

3. Testing procedure

The same testing procedure as described in Ref. [24,36] was followed to conduct all the experiments to ensure identical operating conditions. Once the samples are in position the chamber is sealed and then vacuumed. HFE-7000 is then introduced into the vacuumed chamber. Abundant amount of refrigerant is introduced in the system so that the sample and refrigerant holding cup overflows, this ensures fully lubricated conditions throughout a test. After this the normal load is applied and the experimental control algorithm is initiated. The initial step of the algorithm is the heating of the refrigerant inside the specimen cup. Once the desired refrigerant temperature has been reached, the temperature is maintained and stabilised for 1 h before starting an experiment. After stabilising and maintaining the refrigerant temperature for 1 h a test is run for the duration of 2 h.

The reciprocating frequency is continuously controlled through a driver motor with feedback control. All the transducers, the electric heating elements and the motor are all connected and controlled through a microprocessor based DAQ (data acquisition) and control system. Values obtained by the pressure transducer of the chamber pressure, readings from the two thermocouples, frictional force values from the friction force transducer and the motor speed are constantly logged by using a specialized software COMPEND.

There are in total five different coating that were investigated under identical testing conditions. Three different loads i.e. 10 N, 20 N and 30 N were applied in conjunction with three different refrigerant temperatures of 20 °C, 30 °C and 40 °C. All tests were carried out with a stroke length of 5 mm and a reciprocating frequency of 5 Hz. Repeatability of the results was ensured by performing each test at least two times.

4. Results and discussion

Results of wear and friction have been presented in this study. Each sample pair was studied using SEM to observe the extent and type of wear. EDS analysis was also performed within the contact regions of each flat and ball specimen to investigate the development of tribological films on the top mating surfaces and to gauge the extent of wear on the flat disc samples. After this ZYGO was used to measure the wear volume of the wear scars on the disc samples. The results of wear volume
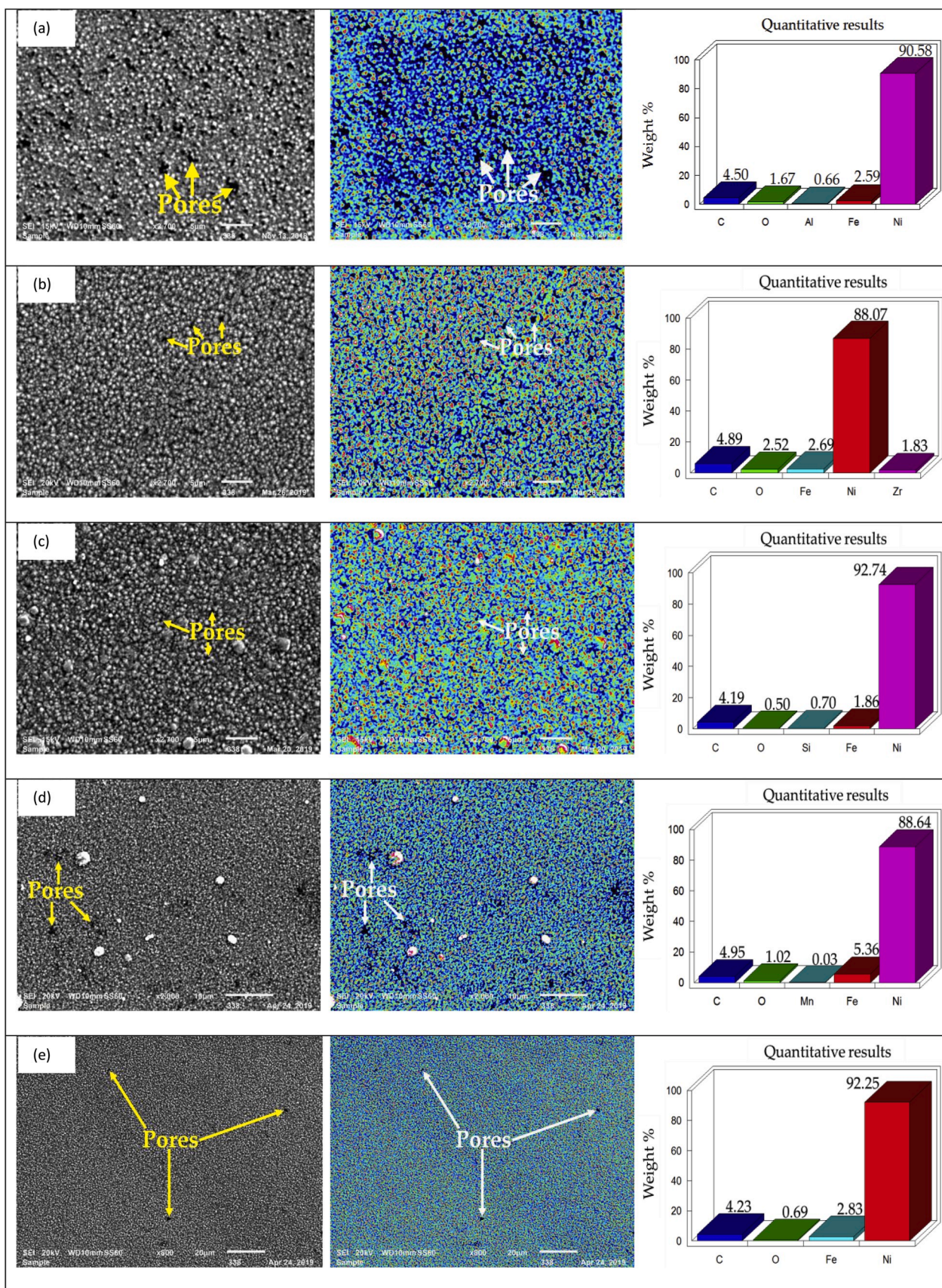
Fig. 1. SEM images and EDS analysis of coated samples; (a) Ni–Al$_2$O$_3$ (b) Ni–ZrO$_2$ (c) Ni–SiC (d) Ni-GPL (e) Pure Nickel.
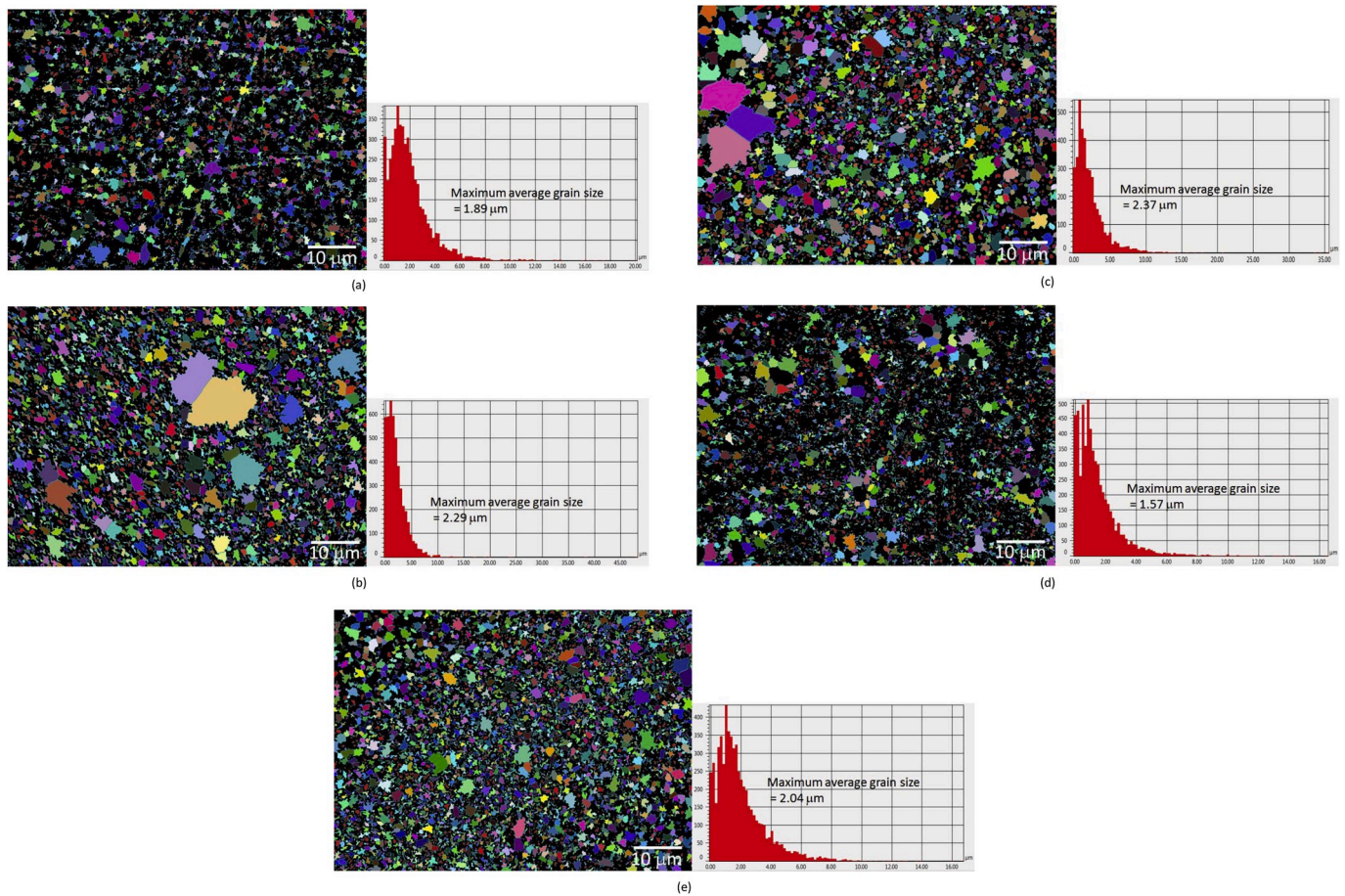
Fig. 2. Pre-test grain size maps: (a) Ni–Al$_2$O$_3$ (b) Ni–ZrO$_2$ (c) Ni–SiC (d) Ni-GPL (e) Nickel-only.

Table 2
Measured mechanical properties of the disc samples.

Specimen	Ni–Al$_2$O$_3$	Ni–ZrO$_2$	Ni–SiC	Ni-GPL	Nickel	Uncoated
Ra (µm)	0.045	0.20	0.18	1.17	0.12	0.10
Hardness (GPa)	3.85 ± 0.28	3.54 ± 0.36	3.84 ± 0.24	3.87 ± 0.38	3.22 ± 0.22	3.00 ± 0.09
Elastic Modulus (GPa)	203.48 ± 11.67	207.17 ± 12.88	247.76 ± 27.24	212.86 ± 15.73	215.94 ± 14.87	212.28 ± 9.32
Mean (H/E) Ratio	0.0189	0.0171	0.0154	0.0182	0.0149	0.0141

of all the coatings were compared to one another and also to an uncoated flat disc sample which was tested under identical operating conditions in our previous study [36]. After this the results of friction are presented as real-time coefficient of friction and average coefficient of friction plots. The coefficient of friction results of each coating were also compared with one another and also to the uncoated steel. This uncoated steel is the steel substrate that was used to apply these coatings. The results highlight and indicate whether or not these coatings are useful for improving the tribological properties of rubbing parts using HFE-7000 refrigerant.

5. Wear

EDS elemental analysis results and SEM micrographs of Ni–ZrO$_2$ are presented in Fig. 4, Fig. 5 and Fig. 6.

Adhesive and abrasive wear mechanism was noted by studying the ball and disc samples under high magnification. A combination of micro-cutting, micro-ploughing and micro-delamination was observed on the worn tracks. For all coatings plastic deformation was apparent due to the higher hardness value of the counter steel ball in comparison to the coatings.

Maximum wear is apparent at lower refrigerant temperature as shown in Fig. 4. With a rise in temperature of the refrigerant to 40 °C from 20 °C the wear scar becomes narrower. EDS elemental analysis of the wear scar at 20 °C reveal only a slight presence of Nickel and a high presence of iron indicating that the coatings have completely worn out. EDS analysis performed on the wear scar also reveal a presence of oxygen and/or fluorine. SEM images of the 52100 steel ball display adhesion of the counter surface on the surface of the steel ball. EDS elemental results of the steel ball in the contact region also confirm adhesion of the delaminated coatings on the hard 52100 steel surface with more adhesion present at 10 N in comparison to higher loads. EDS of the ball samples also demonstrates the presence of oxygen (O) and fluorine (F). Detection of O and F on the steel surfaces indicates formation of surface tribo-films on the mating surfaces. An increase in load at 20 °C refrigerant temperature increases wear; the EDS results of the wear track also reveal a reduced percentage of oxygen and fluorine with increase in load as shown in Fig. 4.

Increasing the refrigerant temperature to 30 °C from 20 °C results in a higher percentage of O and F on the wear scar as shown in Fig. 5. EDS results of the disc samples also show a higher percentage of Nickel and zirconium presence on the wear scar indicating a decrease in wear.
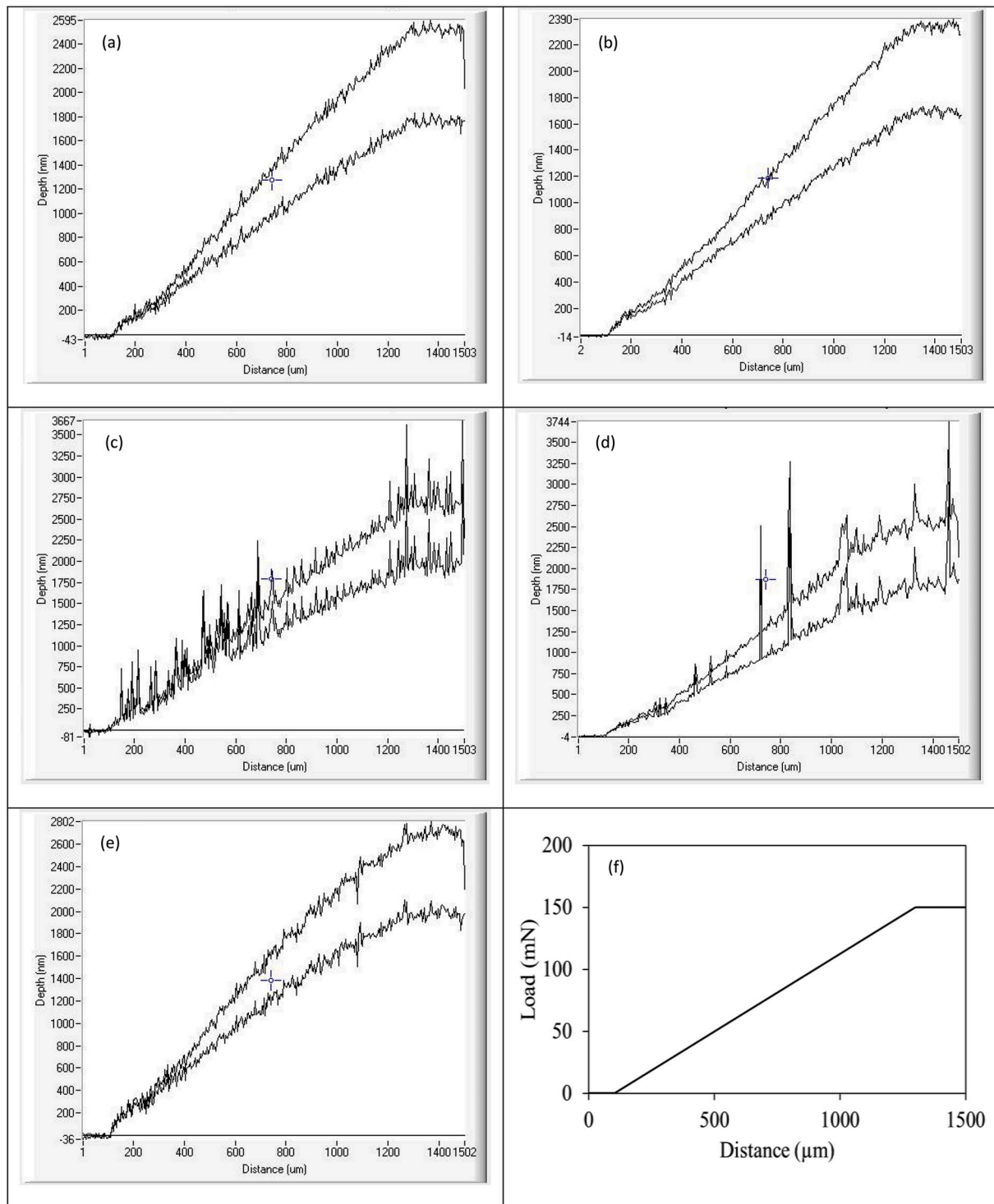
Fig. 3. Scratch Test Results: (a) Ni–Al$_2$O$_3$ (b) Ni–ZrO$_2$ (c) Ni–SiC (d) Ni-GPL (e) Nickel-only (f) Loading profile.

Micrographs of the wear track reveal micro-cutting and micro-delamination of the coated surfaces. SEM images and EDS analysis of the counter steel ball show more adhesion of the coatings on the ball surface in contrast to tests conducted at 20 °C.

Micrographs of the wear track generated by a further rise in the refrigerant temperature to 40 °C from 30 °C show a decrease in wear track width and overall wear as shown in Fig. 6. This is also visible from the EDS results; which reveal a significant presence of Nickel and zirconium in comparison to the tests conducted at 20 °C and 30 °C. EDS analysis also reveal a higher percentage of F and O on the disc as well as

the ball surfaces in comparison to the tests conducted at a lower temperatures.

The micrographs of the ball and flat specimens indicate that wear occurred primarily due to micro cutting at 20 °C refrigerant temperature, micro-delamination was the dominant wear phenomenon at 30 °C and a mix of micro-cutting and micro-delamination occurred at 40 °C.

The SEM images and the EDS results of the tests conducted on Ni–SiC nanocomposite coatings are presented in Figs. 7–9. Fig. 7 shows the results of all the tests conducted at 20 °C refrigerant temperature. The micrographs show micro-cutting and micro-delamination of Ni–SiC
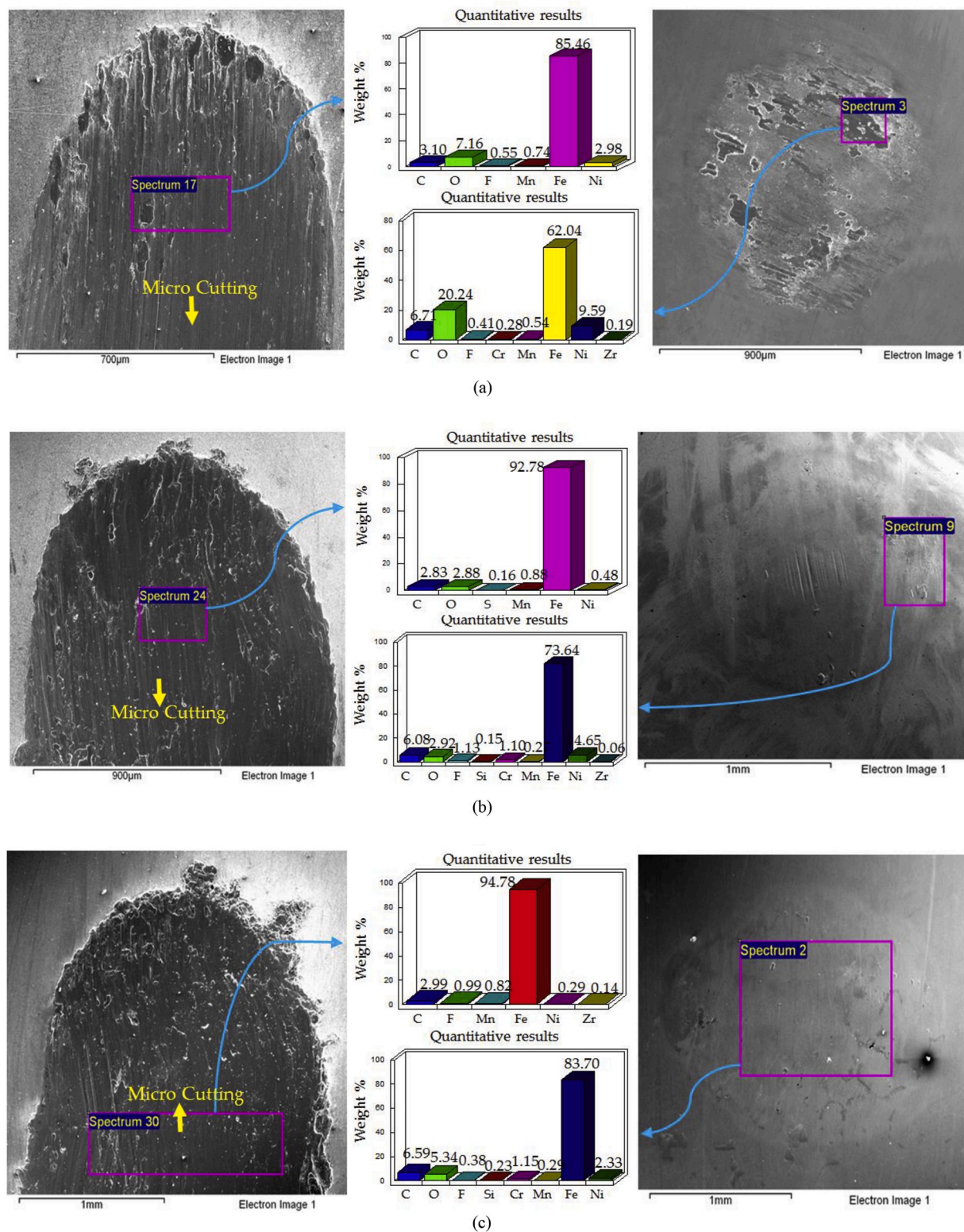
Fig. 4. EDS elemental results and SEM Micrographs of Ni–ZrO₂ coated flat samples and counter steel ball: (a) 20 °C, 10 N (b) 20 °C, 20 N (c) 20 °C, 30 N.

coatings. At refrigerant temperature 20 °C, wear has occurred due to micro-cutting and micro-delamination at 10 N and 20 N, increase in load to 30 N at 20 °C shifts the mechanism more towards micro-cutting as shown in Fig. 7. An increase in the temperature of the refrigerant from 20 °C to 30 °C shows a decrease in wear and a shift in wear mechanism towards micro-cutting as shown in Fig. 8. An increase in refrigerant temperature also results in more adhesion of the worn coatings onto the

steel ball. EDS results also show a higher presence of Nickel on the top surfaces at 30 °C refrigerant temperature in comparison to tests conducted at 20 °C.

An additional increase in the temperature of the refrigerant from 30 °C to 40 °C reduces the severity of wear. As shown in Fig. 9 micro-delamination and micro-cutting is observed on the wear track at 40 °C/10 N; while micro-ploughing and micro-delamination is apparent at
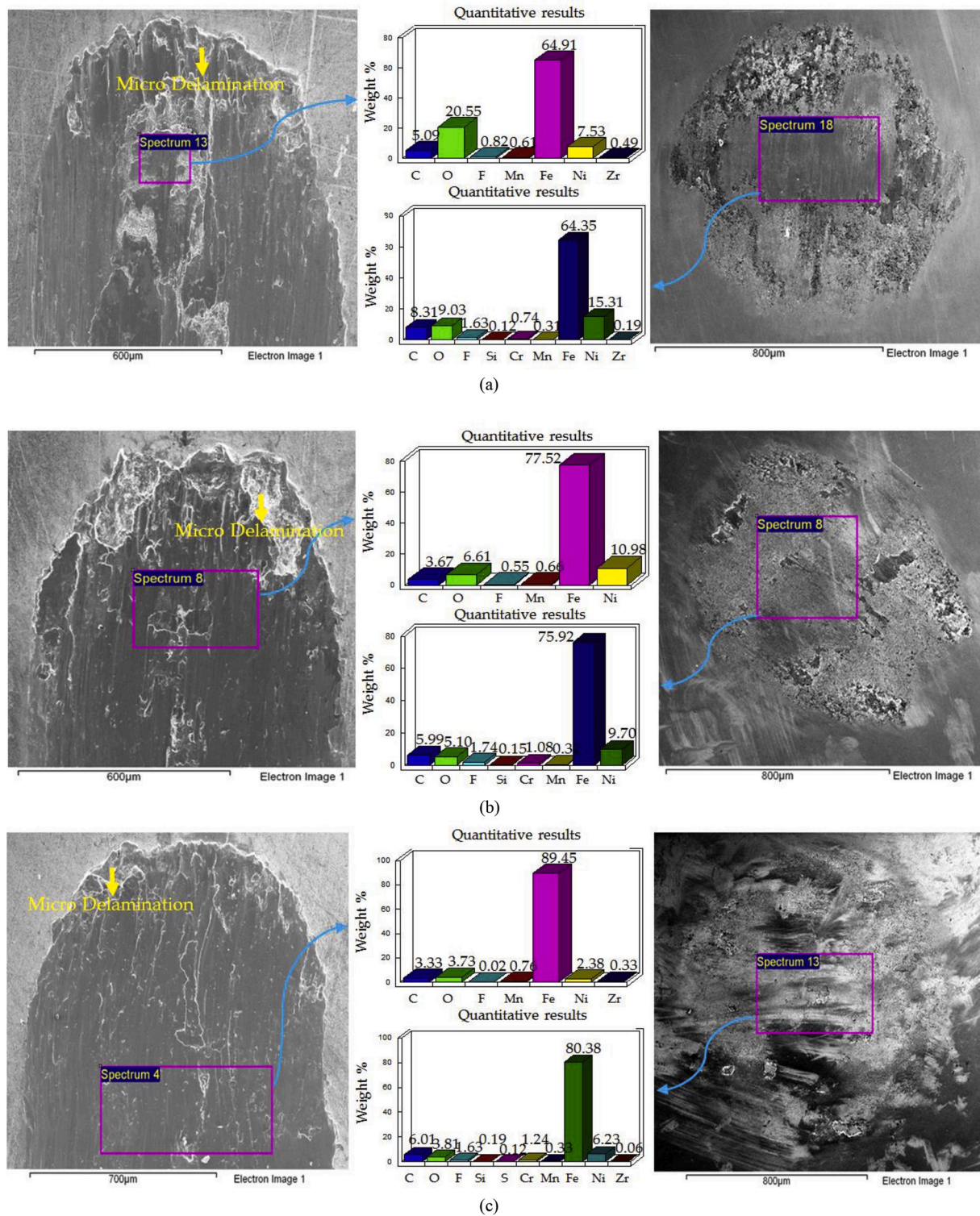
Fig. 5. EDS elemental results and SEM Micrographs of Ni–ZrO₂ coated flat samples and counter steel ball: (a) 30 °C, 10 N (b) 30 °C, 20 N (c) 30 °C, 30 N.

40 °C/20 N and 40 °C/30 N. Adhesion of the coatings is also visible on the counter steel ball at the tests conducted at 40 °C.

EDS analysis on the wear scar show a higher percentage of Nickel and silicon on the flat disc implying the presence of the nanocomposite coatings and a reduction in wear.

High magnification images and EDS results of Ni–Al₂O₃ are presented in Figs. 10–12. At 20 °C, increase in load increased wear. Delamination of the coatings occurred at 20 °C/20 N and 20 °C/30 N

which is evident from the micrographs and EDS results shown in Fig. 10. At 20 °C/10 N and 20 °C/30 N testing conditions micro-delamination and micro cutting resulted in the wear of the disc sample. SEM images at 20 °C/20 N testing conditions present micro-cutting to be the main cause of wear.

Increasing the temperature of the refrigerant to 30 °C had a significant positive impact on reducing wear at 20 N as shown in Fig. 11. Complete coating delamination was not observed at 30 °C/20 N. Results
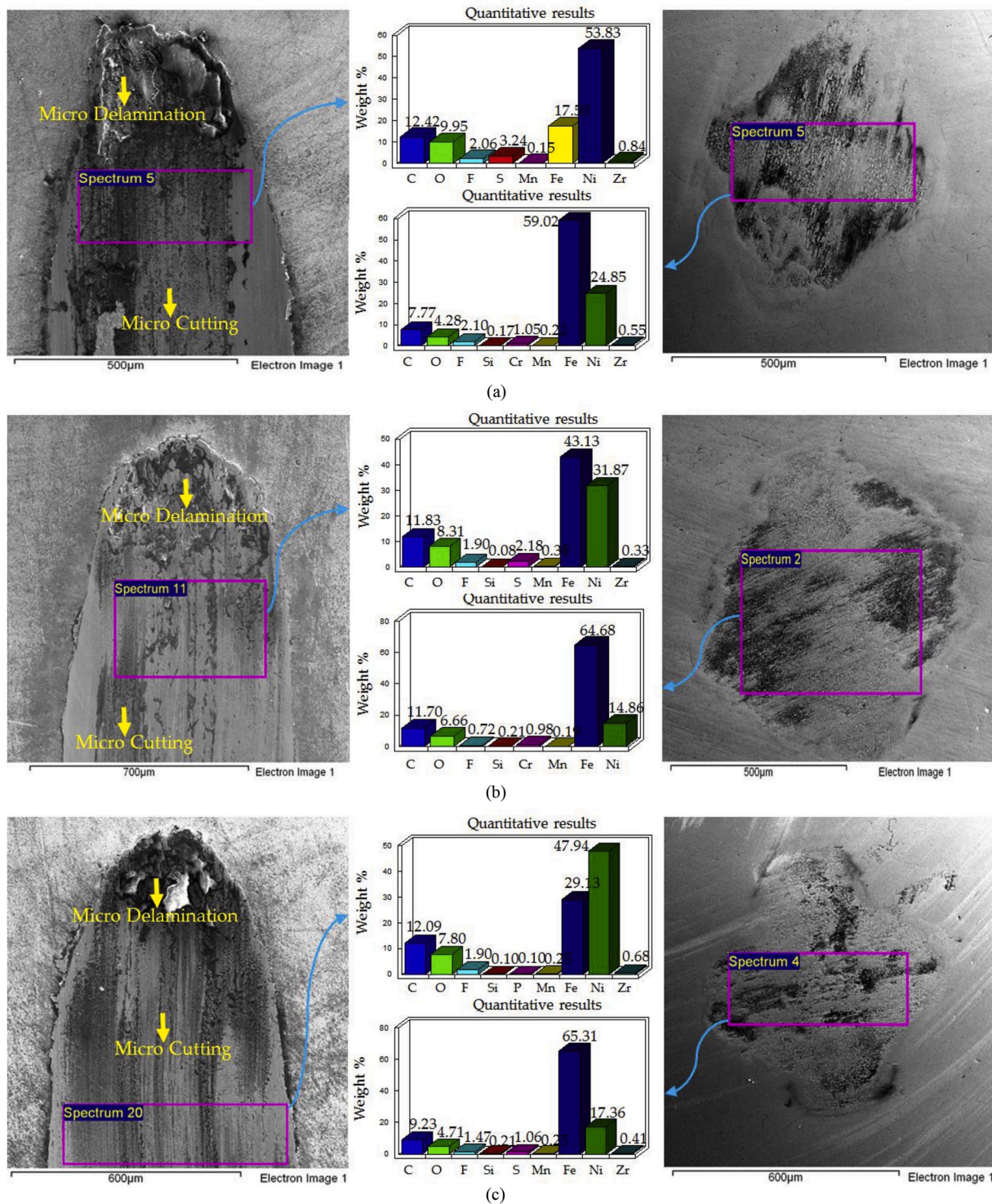
Fig. 6. EDS elemental results and SEM Micrographs of Ni–ZrO$_2$ coated flat samples and counter steel ball: (a) 40 °C, 10 N (b) 40 °C, 20 N (c) 40 °C, 30 N.

at 30 °C/30 N were analogous to the results obtained at 20 °C/30 N. The coating delaminated completely at 30 °C/30 N as well. Results at 30 °C/10 N were different in terms of wear phenomenon; micro-delamination is the more governing wear mechanism at 20 °C/10 N whereas wear primarily due to micro-cutting can be observed at 30 °C/10 N.

Results of increasing the refrigerant temperature to 40 °C from 30 °C have been displayed in Fig. 12. At 40 °C/10 N a combination of micro-delamination and micro-cutting can be observed. EDS analysis of all the tests carried out at normal load of 10 N show a significance presence of Nickel along with aluminium indicating that Ni–Al$_2$O$_3$ coatings did not

totally wear out at low loads. Micro-cutting can be observed on the wear scar with an increase in load at 40 °C to 20 N. An additional increase load to 30 N at 40 °C resulted in micro-cutting and micro-delamination. EDS examination of the wear scars at 40 °C on all the disc samples showed a significance presence of Nickel which shows that at higher refrigerant temperatures wear has been reduced.

EDS elemental analysis results and SEM Micrographs of the tests conducted on Nickel-Graphene (Ni-GPL) coatings have been presented in Figs. 13–15. SEM images at refrigerant temperature 20 °C at any given applied load show high wear and the results reveal Ni-GPL coatings to be
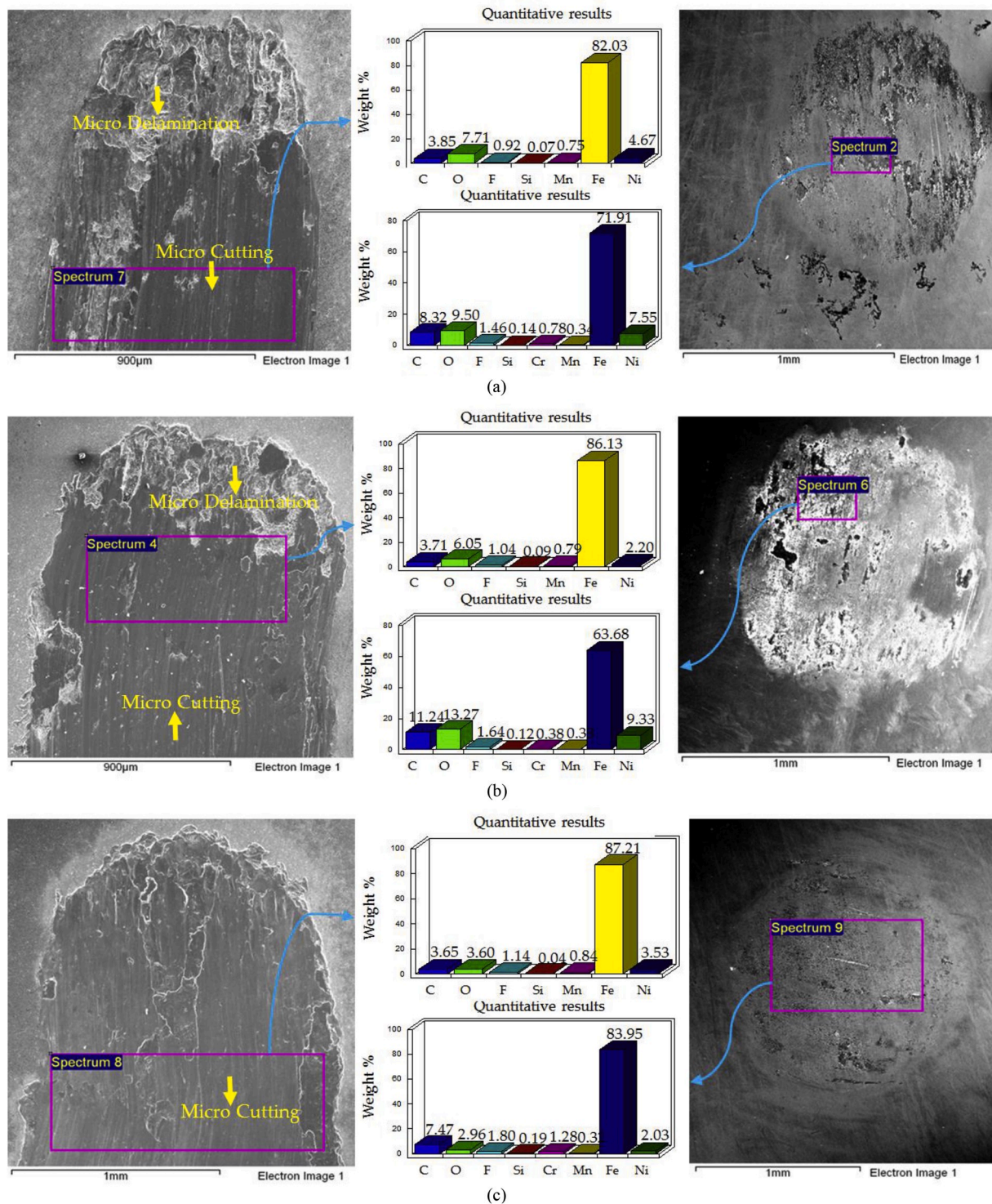
Fig. 7. EDS elemental results and SEM Micrographs of Ni–SiC coated flat samples and counter steel ball: (a) 20 °C, 10 N (b) 20 °C, 20 N (c) 20 °C, 30 N.

completely worn out mainly due to micro-cutting as presented in Fig. 13.

Increasing the refrigerant temperature to 30 °C from 20 °C at 10 N load results in lesser damage and micro-ploughing can be observed on the wear track at 30 °C/10 N as shown in Fig. 14. At 30°/20 N and 30°/30 N a mix of micro-ploughing and micro-delamination can be observed. EDS results at 30°for all the loads show a higher presence of Nickel in comparison to the tests conducted at 20 °C, this indicates a reduction in wear by an increase in refrigerant temperature.

Micro-cutting and micro-delamination can be observed at 40 °C/10 N and 40 °C/30 N while wear primarily due to micro-ploughing and

micro-delamination took place at 40 °C/20 N as shown in Fig. 15. EDS results at 40 °C/10 N present the highest percentage of Nickel amongst all the tests that were conducted on Ni-GPL. EDS on the wear track of all the disc samples at 40 °C show a higher percentage of Nickel at any given load in contrast to tests conducted at lower refrigerant temperatures. This shows a decrease in wear when using Ni-GPL coatings by increasing the temperature to 40 °C from 20 °C. Increase in the temperature of the refrigerant to 40 °C from 20 °C also results in an increase in adhesion of the coatings on the steel ball.

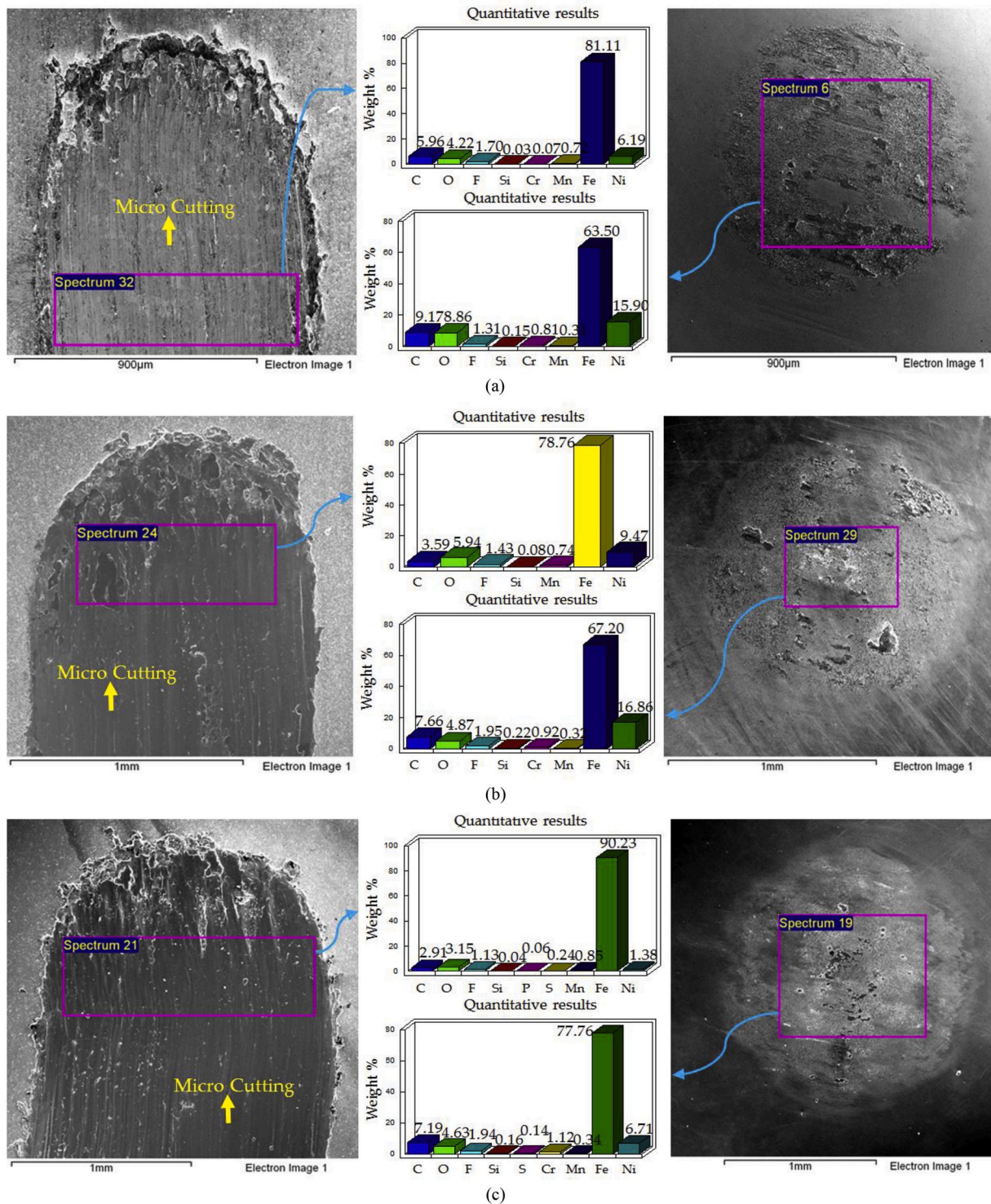High magnification images and EDS examination of Nickel-only

Fig. 8. EDS elemental results and SEM Micrographs of Ni–SiC coated flat samples and counter steel ball: (a) 30 °C, 10 N (b) 30 °C, 20 N (c) 30 °C, 30 N.

coated samples are displayed in Figs. 16–18. Tests conducted at 20 °C refrigerant temperature show wear primarily due to micro-cutting and micro-delamination as shown in Fig. 16. EDS analysis show only a small percentage of Nickel on the wear track indicating high wear at low refrigerant temperature. Micro-delamination is more prominent at 20 °C/10 N and micro-cutting is more dominating wear mechanism at 20 °C/30 N.

EDS results of increasing the temperature of the refrigerant to 30 °C presented in Fig. 17 show a higher presence of Nickel in comparison to

the tests conducted at 20 °C which shows a decrease in wear by increase in temperature. Wear at 30 °C is also mainly due to micro-cutting and micro-delamination. Wear at 30 °C/20 N is mainly due to micro-cutting whereas wear occurs due to a mix of micro-delamination and micro-cutting at 30 °C/10 N and 30 °C/30 N.

EDS results at 40 °C presented in Fig. 18 reveal an even higher percentage of Nickel at any given load on the wear track implying a further reduction in wear by increasing the temperature of the refrigerant. 40 °C/10 N and 40 °C/20 N operating conditions show wear due
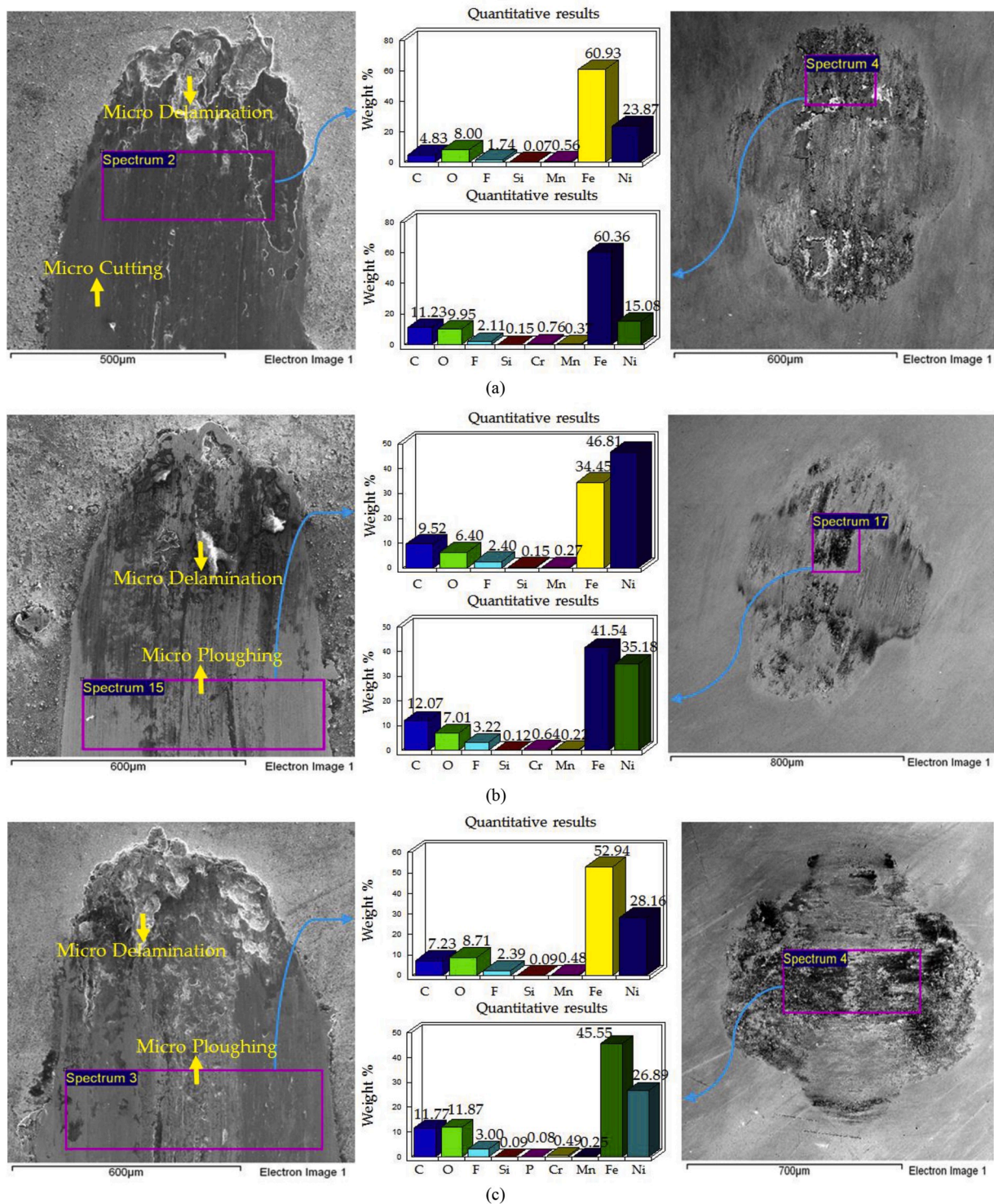
Fig. 9. EDS elemental results and SEM Micrographs of Ni–SiC coated flat samples and counter steel ball: (a) 40 °C, 10 N (b) 40 °C, 20 N (c) 40 °C, 30 N.

to micro-delamination and micro-cutting; whereas wear at 40 °C/30 N occurred due to micro-ploughing.

5.1. Wear volume

The wear scar produced on each disc sample was studied under ZYGO to measure the wear volume of the wear track. Each wear scar was stitched to generate a 3D plot of the complete wear track. Results of Ni–ZrO$_2$ obtained from the interferometer have been presented in Fig. 19. Similar wear profiles were obtained for the other coatings as

well. Wear volume was measured using the 3D plots and the interferometer.

Results of wear of the uncoated flat samples having R$_a$ of 0.1 μm from our previous study [36] have been presented in Fig. 20 for reference. Wear volume produced on each coated sample was compared to the uncoated samples to study the effect of using Nickel based nano-composite coatings in comparison to non-coated specimens. Fig. 21 shows the wear volume plot of Ni–ZrO$_2$ nanocomposite coatings and the percentage effect in wear volume by the application of Ni–ZrO$_2$ on a steel substrate in comparison to uncoated steel. At a lower refrigerant
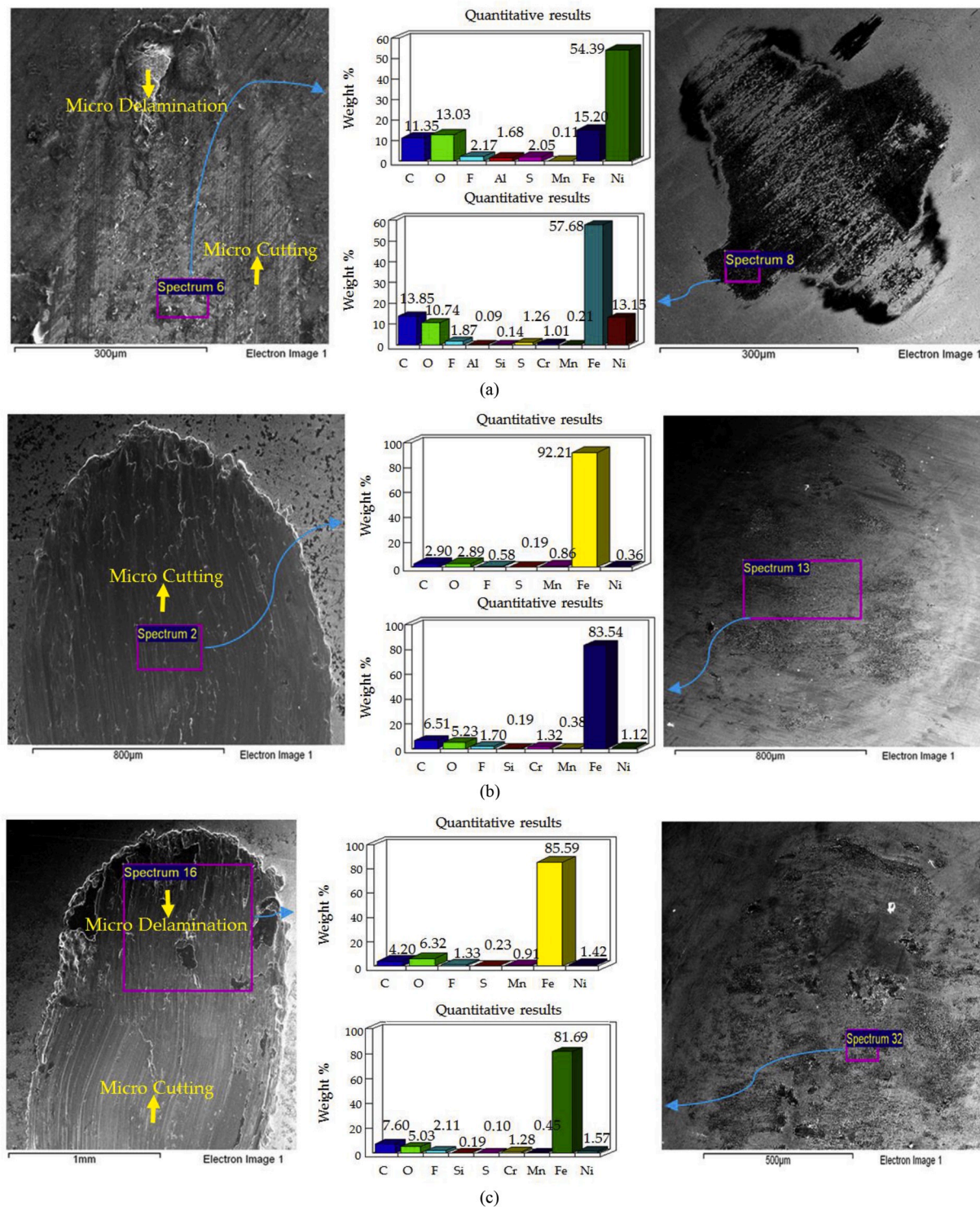
Fig. 10. EDS elemental results and SEM Micrographs of Ni–Al$_2$O$_3$ coated flat samples and counter steel ball: (a) 20 °C, 10 N (b) 20 °C, 20 N (c) 20 °C, 30 N [24].

temperature of 20 °C, an increase in load increases the wear volume. Increasing the refrigerant temperature to 30 °C generates almost the same amount of wear as 20 °C at 10 N load, however at higher loads i.e. 20 N and 30 N; there is a very significant drop in wear volume in comparison to wear at 20 °C. Interestingly for 30 °C refrigerant temperature, least amount of wear was generated at 20 N load and 10 N load resulted in maximum wear. An additional increase in temperature by 10 °C dropped wear even further and it can be seen from the results that least amount of wear occurred at 40 °C at any given load for Ni–ZrO$_2$

coatings. This drop in wear with rise in temperature is due to the formation oxygenated and fluorinated anti-wear tribo-films on the top surfaces of the mating parts. EDS analysis show a clear presence of O and F on the wear scar as well as the counter steel ball. EDS results also show an increase in the percentage of oxygen and fluorine on the wear scar with rise in refrigerant temperature to 40 °C from 20 °C. Overall least amount of wear was observed at 40 °C/20 N.

Wear volume generated by using Ni–ZrO$_2$ nanocomposite coatings at each testing condition was also compared to the uncoated steel sample.
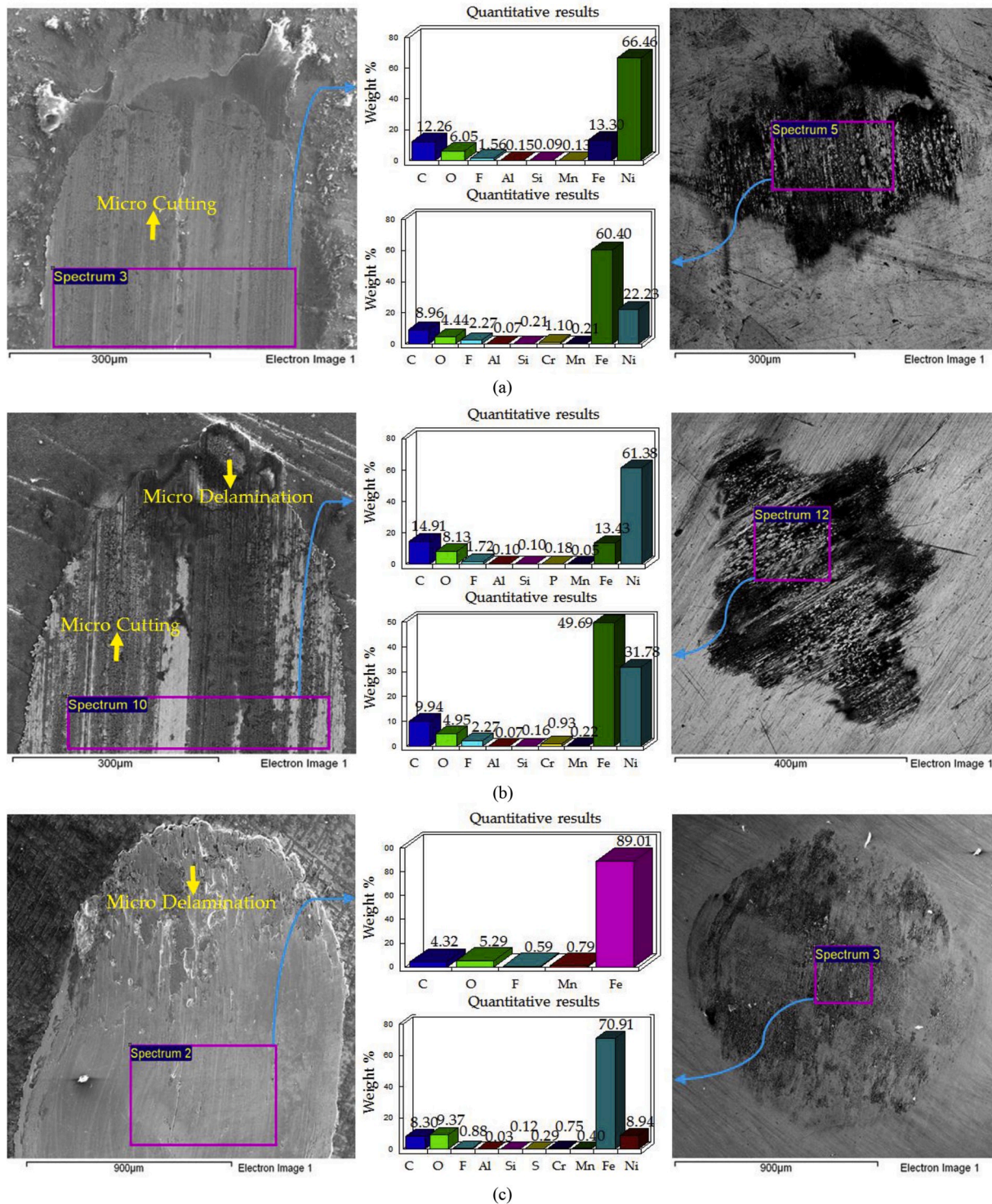
Fig. 11. EDS elemental results and SEM Micrographs of Ni–Al$_2$O$_3$ coated flat samples and counter steel ball: (a) 30 °C, 10 N (b) 30 °C, 20 N (c) 30 °C, 30 N.

Percentage wear volume change by using Ni–ZrO$_2$ show a clear decrease in wear volume at all the testing conditions. Improvement in wear reduction is less at lower refrigerant temperature of 20 °C and maximum wear reduction occurs at higher refrigerant temperature of 40 °C. Minimum wear improvement was observed at 20 °C/20 N testing conditions, SEM images and EDS results at these conditions show high wear due to micro-cutting and almost complete wear out of the coatings. A combination of micro-cutting and micro-delamination of the coatings at 30 °C/ 10 N also produce high wear which results in the least improvement in

wear at 30 °C. At 40 °C refrigerant temperature wear decreases by over 70% for 10 N and 30 N loads; at 40 °C/20 N the improvement was just below 65%. Both the uncoated steel and Ni–ZrO$_2$ coated samples showed best wear results at 40 °C/20 N, this indicates that exists an optimal temperature and load combination that generates best wear performance when using HFE-7000.

Compared to the uncoated steel, there is an improvement in the micro-hardness and H/E ratio by applying Ni–ZrO$_2$ coatings which improved the wear performance of interacting parts under reciprocating
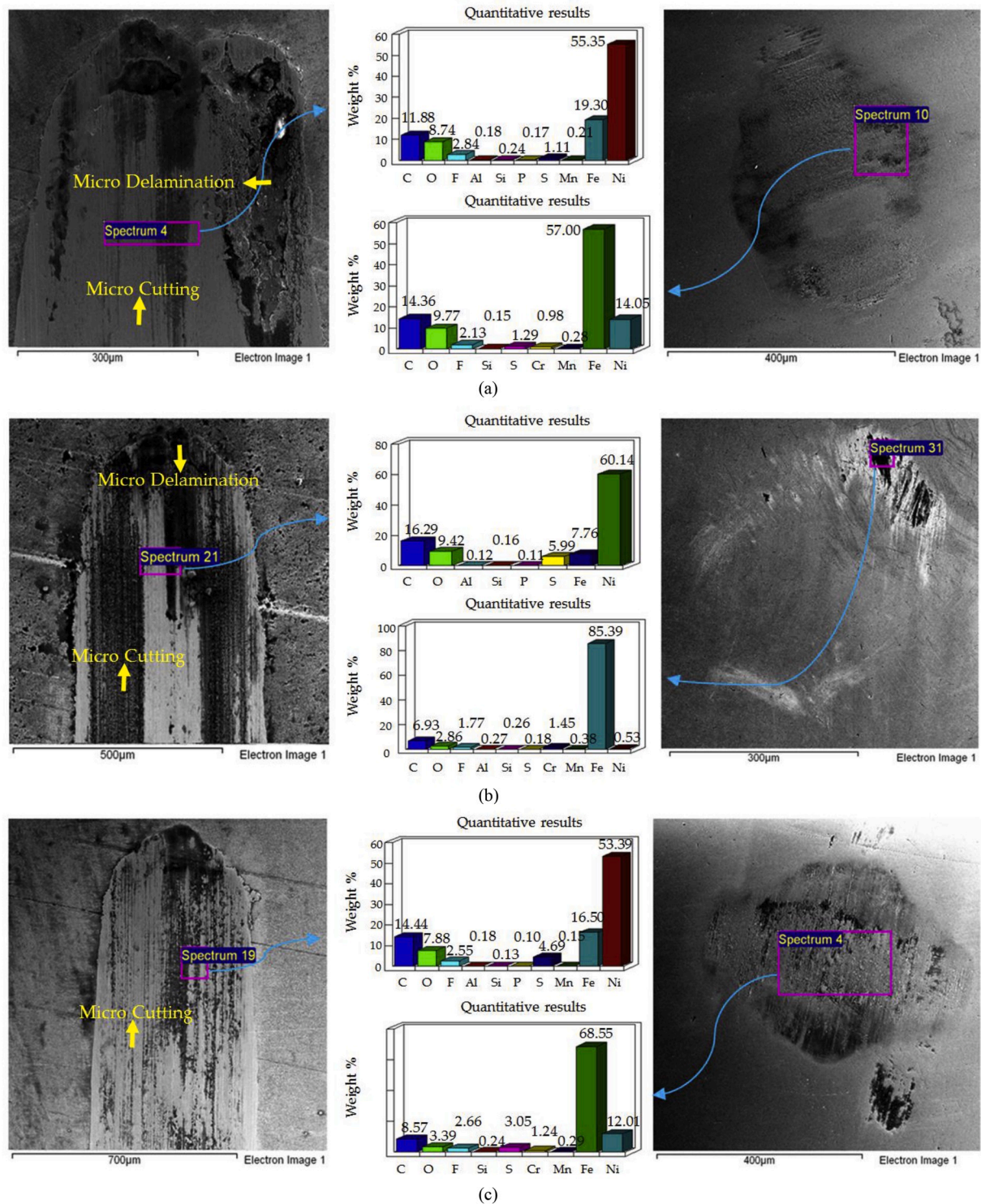
Fig. 12. EDS elemental results and SEM Micrographs of Ni–Al$_2$O$_3$ coated flat samples and counter steel ball: (a) 40 °C, 10 N (b) 40 °C, 20 N (c) 40 °C, 30 N [24].

motion.

Results of wear volume produced by applying Ni–SiC nanocomposite coatings on the steel substrate have been presented in Fig. 22. At temperatures of 20 °C and 30 °C, increase in load generates higher wear. A reduction in wear is witnessed by increasing the temperature of the refrigerant from 20 °C to 30 °C. Wear reduces further by an increase in the temperature of the refrigerant to 40 °C. This drop in wear volume with increase in refrigerant temperature is linked with the formation of oxygen and fluorine containing tribo-films on the top surfaces.

Similar to uncoated steel and Ni–ZrO$_2$ coated steel samples, minimum wear occurs at 40 °C/20 N for Ni–SiC coated samples as well. EDS results show an increase in the content of fluorine and oxygen on the wear scar indicating an accelerated formation of protective surface films. Comparing wear produced by using Ni–SiC nanocomposite coatings to the uncoated steel show a clear reduction in wear volume. Similar to Ni–ZrO$_2$, Ni–SiC coatings also produced the least positive effect at 20 °C/20 N. High wear occurred at 20 °C/20 N due to microdelamination and micro-cutting at these testing conditions. In contrast
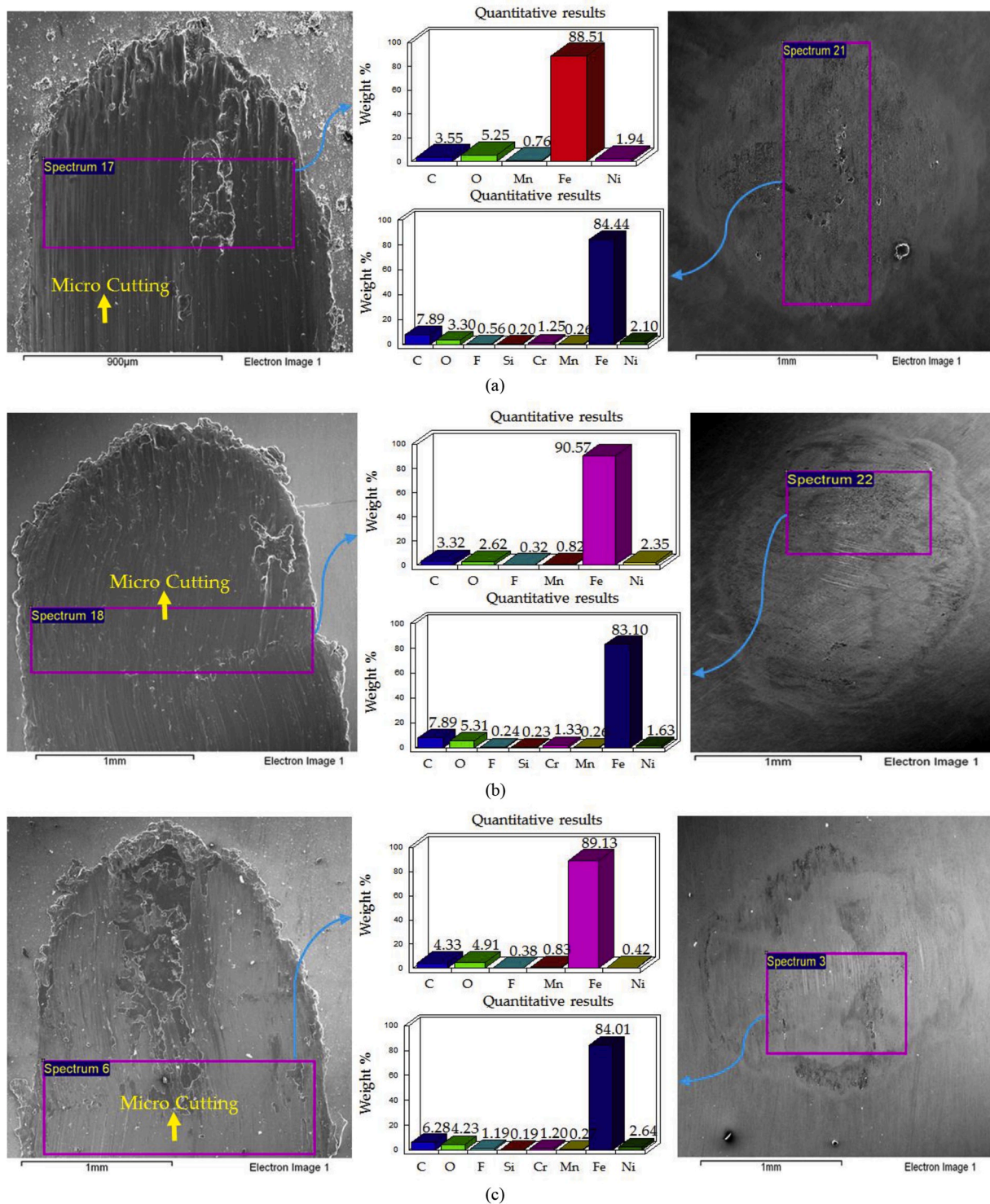
Fig. 13. EDS elemental results and SEM Micrographs of Ni-GPL coated flat samples and counter steel ball: (a) 20 °C, 10 N (b) 20 °C, 20 N (c) 20 °C, 30 N.

to Ni–ZrO$_2$ coatings at which 10 N load resulted in the highest wear drop, 30 N load proved to be more beneficial for Ni–SiC at 20 °C refrigerant temperature. At refrigerant temperatures of 30 °C and 40 °C, increase in load produced a higher percentage drop in wear volume by applying Ni–SiC coatings when compared to uncoated steel. Ni–SiC coatings improved the micro-hardness of the surface and had the third best hardness amongst the coatings produced. (H/E) ratio also improved by applying Ni–SiC coatings in comparison to the steel substrate. An enhancement in the mechanical properties improved the wear resistance

of the coatings and resulted in a decrease in wear.

Wear volume results of Ni–Al$_2$O$_3$ nanocomposite coatings have been presented in Fig. 23. The very first testing condition of 20 °C/10 N show a very significant drop in wear volume as compared to uncoated steel and also in comparison to Ni–ZrO$_2$ and Ni–SiC. Percentage wear volume change by applying Ni–Al$_2$O$_3$ coatings when compared to uncoated steel show remarkable improvement in wear loss and a drop in wear by over 92%. Ni–Al$_2$O$_3$ nanocomposite coatings showed the second best hardness and the best (H/E) ratio as compared to all the other samples. This
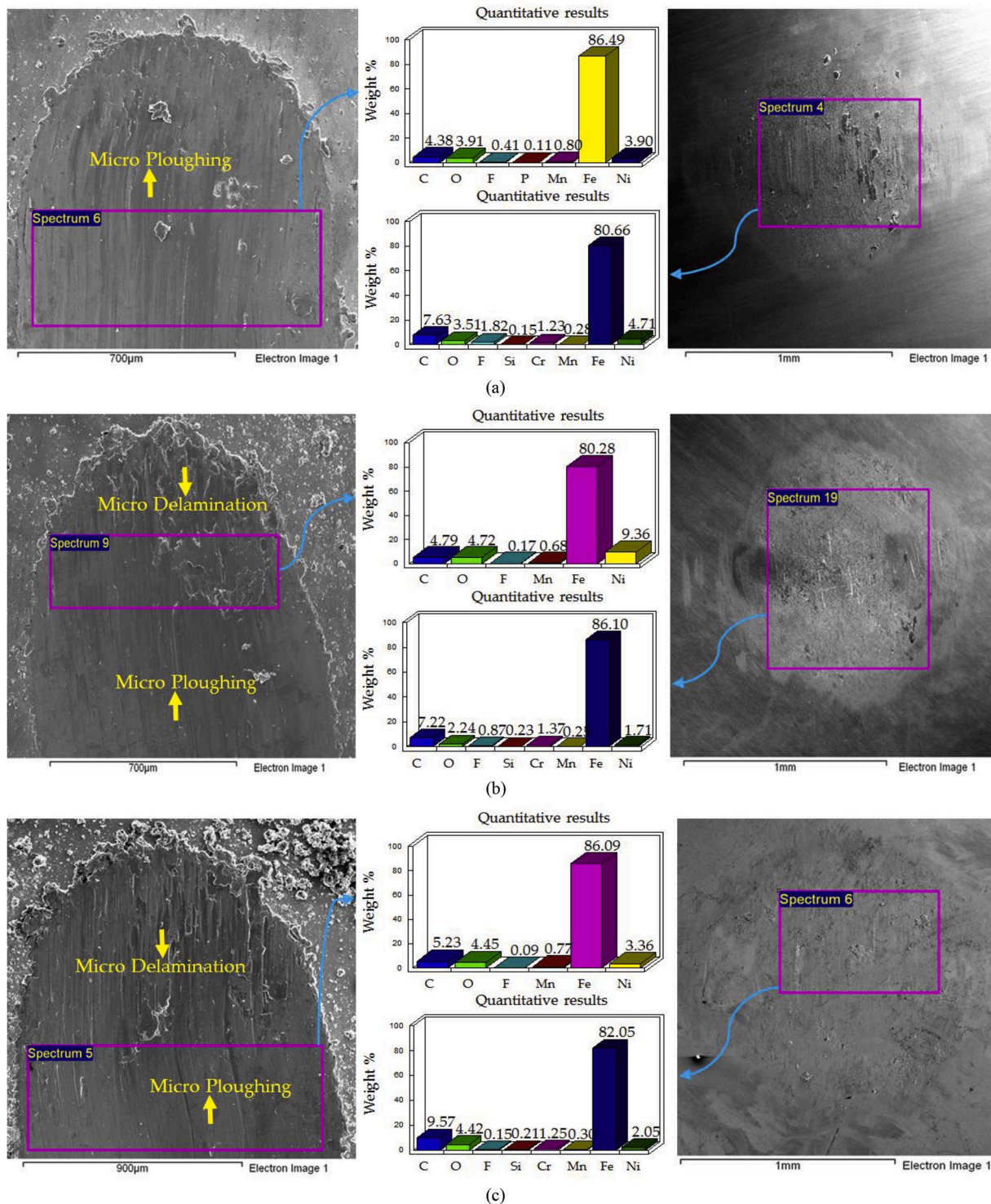
Fig. 14. EDS elemental results and SEM Micrographs of Ni-GPL coated flat samples and counter steel ball: (a) 30 °C, 10 N (b) 30 °C, 20 N (c) 30 °C, 30 N.

improvement in mechanical properties provides better wear resistance which reduces wear significantly. Increasing the applied normal load to 20 N at 20 °C generates significant wear. Percentage wear volume change graph also shows an increase in wear at 20 °C/20 N by applying Ni–Al$_2$O$_3$ coatings. This shift in wear is due to the delamination of these coatings from the steel substrate by increasing load. Constant oscillating/reciprocating motion has been known to delaminate Ni–Al$_2$O$_3$ coatings [24,34]. Delamination of Ni–Al$_2$O$_3$ coatings from the steel substrate is also evident from the micrographs presented in Fig. 10. As

observed with the other coatings, increasing the applied normal load to 30 N at 20 °C further increases wear. Comparing the results of wear of Ni–Al$_2$O$_3$ coatings with uncoated steel show an improvement in wear loss. Although a complete delamination of the coatings is also observed at 20 °C/30 N similar to 20 °C/20 N, however more O and F were present on the wear scar at 30 °C/30 N in contrast to 20 °C/20 N; which indicates a higher presence of tribo-films which play a key role in reducing wear.

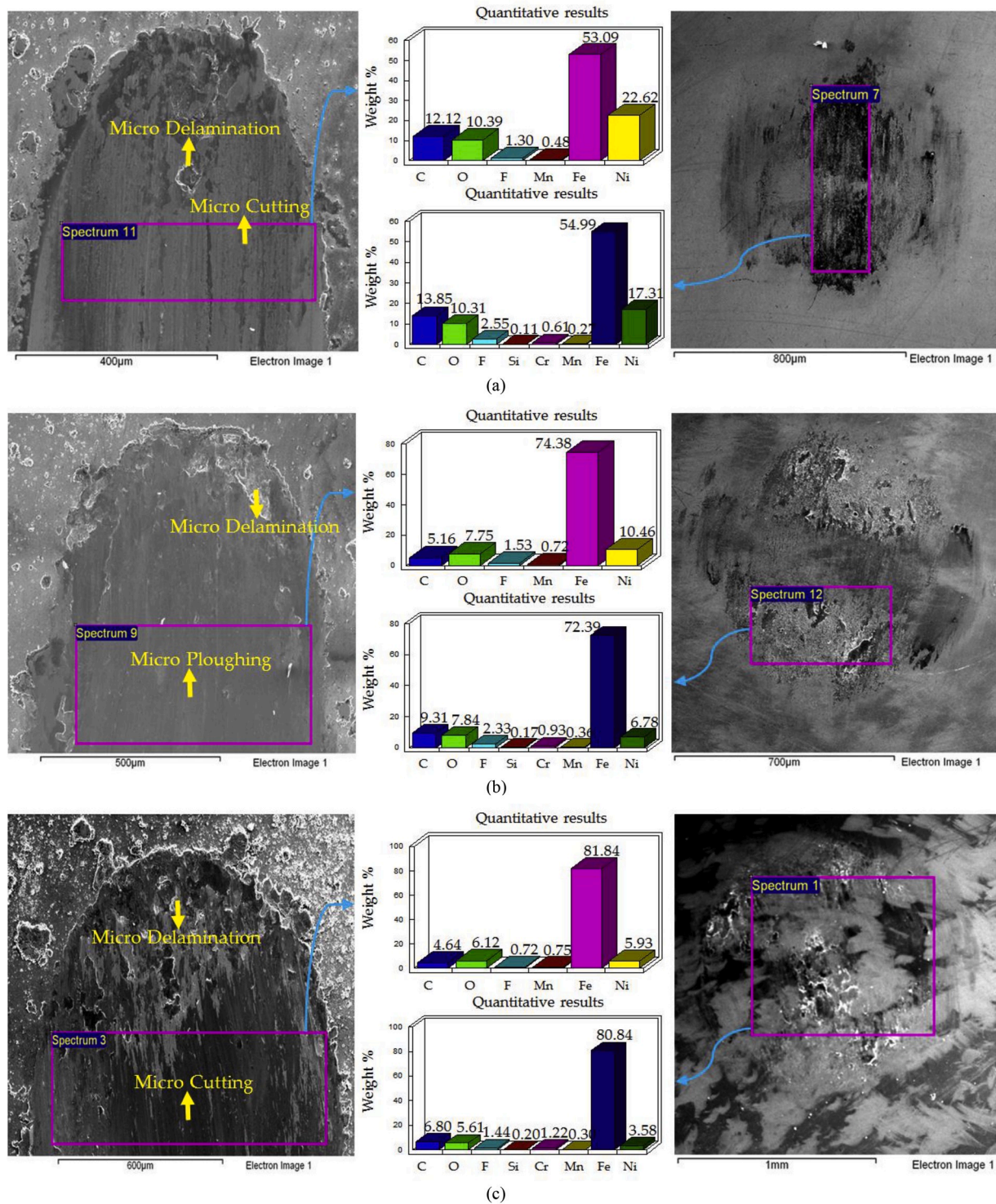Wear volume decreases by increasing the temperature of the

Fig. 15. EDS elemental results and SEM Micrographs of Ni-GPL coated flat samples and counter steel ball: (a) 40 °C, 10 N (b) 40 °C, 20 N (c) 40 °C, 30 N.

refrigerant to 30 °C from 20 °C at any given load by applying Ni–Al₂O₃ nanocomposite coatings. 30 °C/10 N testing conditions also result in a very significant decline in wear, in comparison to uncoated steel wear decreases by over 93% by using Ni–Al₂O₃ coatings at these operating conditions. Unlike 20 °C/20 N testing conditions, the tests conducted at 30 °C/20 N reduced wear and when comparing to uncoated steel wear volume decreased by over 77% at 30 °C/20 N. 30 °C/30 N test also produced a different result in contrast to 20 °C/30 N, wear volume decreased at 20 °C/30 N whereas wear increased at 30 °C/30 N in comparison to uncoated steel. SEM images presented in Fig. 11 show

complete delamination of these coatings at 30 °C/30 N which results in higher wear. Results at 40 °C refrigerant temperature were similar to the results obtained at 20 °C, wear reduction was observed at 10 N and 30 N whereas increase in wear occurred at 20 N. Compared to uncoated steel wear volume decreased by more than 90% at 40 °C/10 N and more than 78% at 40 °C/30 N. The micrographs and EDS analysis results as presented in Fig. 12 show a significant presence of Nickel at 40 °C/20 N showing that the coating has not worn out but still compared to the uncoated test conducted at 40 °C/20 N the amount of wear produced is more by employing Ni–Al₂O₃ coatings in comparison to uncoated steel.
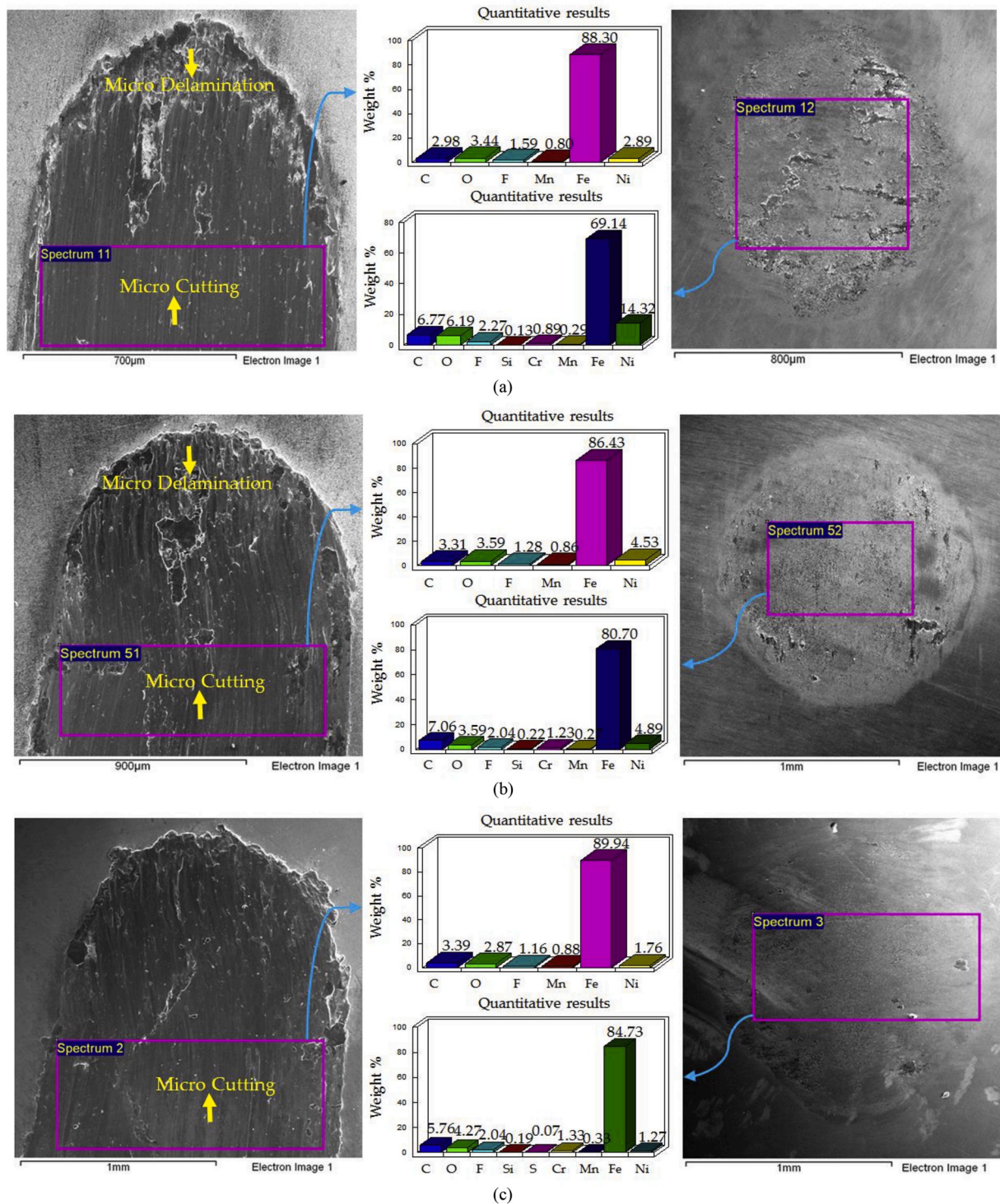
Fig. 16. EDS elemental results and SEM Micrographs of Nickel-only coated flat samples and counter steel ball: (a) 20 °C, 10 N (b) 20 °C, 20 N (c) 20 °C, 30 N.

The reason for higher wear production at 40 °C/20 N by applying Ni–Al$_2$O$_3$ coating is because 40 °C/20 N condition was the most optimum testing condition which produced least amount of wear with uncoated steel. A higher percentage of oxygen and fluorine was also present on uncoated steel samples in contrast to Ni–Al$_2$O$_3$ coated samples at 40 °C/20 N [24] which highlights the significance of oxygenated and fluorinated films in reducing wear. Compared to the other coatings and the uncoated sample, Ni–Al$_2$O$_3$ coated samples at 40 °C/20 N did not result in minimum wear. Minimum wear for Ni–Al$_2$O$_3$ coated samples was observed at 30 °C/10 N.

Wear volume results by using Ni-GPL have been presented in Fig. 24. Ni-GPL coatings had the best hardness values and the second best (H/E) ratio amongst all the coatings produced in this study. The results however show a totally different pattern by using Ni-GPL at 20 °C refrigerant temperature compared to the rest of the coatings. Maximum wear at 20 °C is observed at 20 N instead of 30 N. Wear volume produced at 20 °C/ 10 N and 20 °C/20 N is considerably high, both of these testing conditions when using Ni-GPL coatings have an adverse effect on wear and wear volume has increased drastically. Ni-GPL coatings at these conditions have completely worn out and EDS results on the wear track at 20
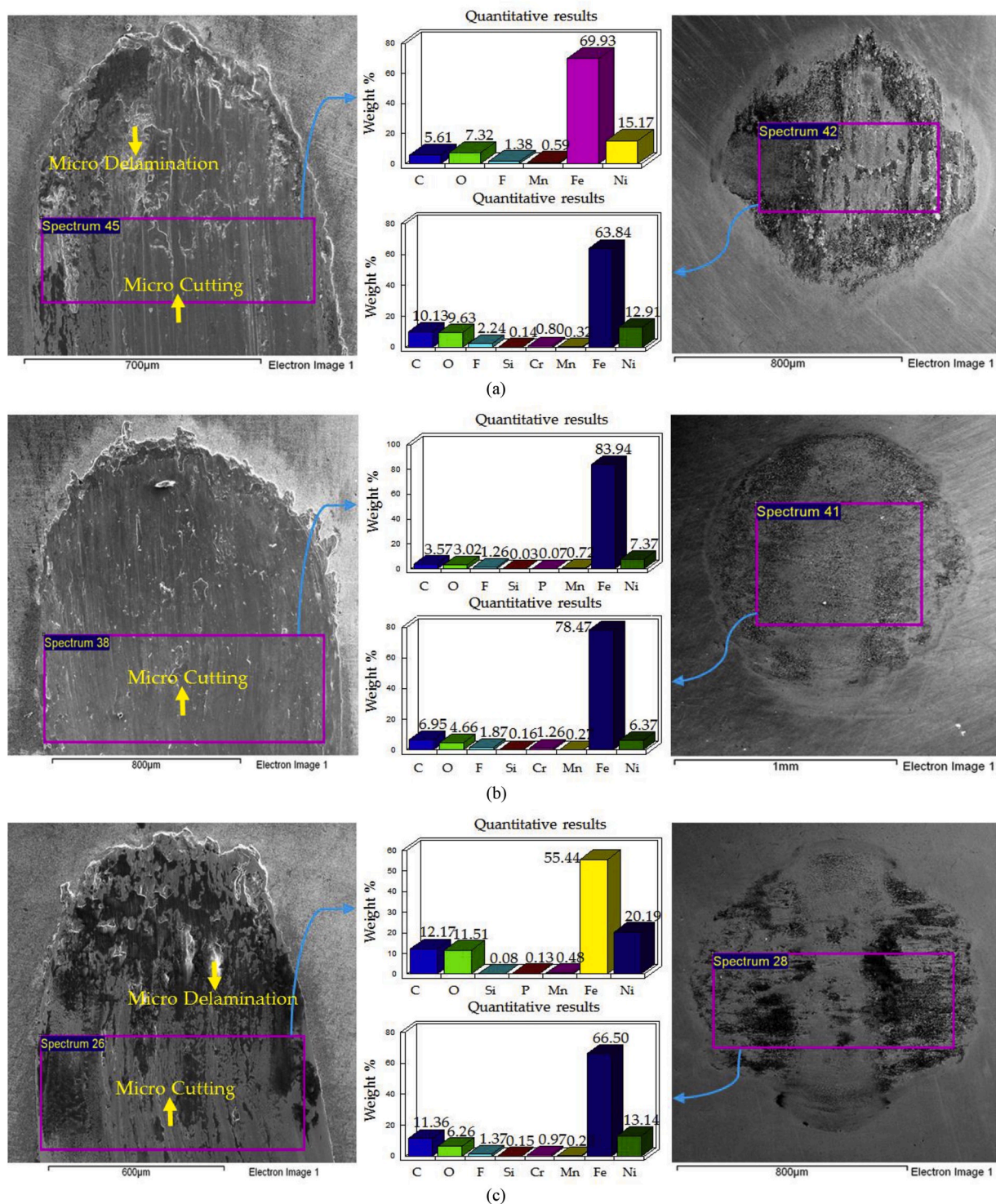
Fig. 17. EDS elemental results and SEM Micrographs of Nickel-only coated flat samples and counter steel ball: (a) 30 °C, 10 N (b) 30 °C, 20 N (c) 30 °C, 30 N.

°C/10 N show no fluorine and at 20 °C/20 N only a very small percentage of oxygen and fluorine was detected as shown in Fig. 13. This shows extreme wear and a very minor presence of anti-wear tribo-films under these conditions. Comparing uncoated steel with Ni-GPL shows an increase in wear by over 67% at these conditions. This high wear when using Ni-Graphene is believed to be because of two reasons.

The first reason is most probably the incompatibility of HFE-7000 with Graphene based Nano coatings. HFE-7000 has a chemical formula $C_3F_7OCH_3$, Carbon–Fluorine (C–F) single bonds are highly polar bonds and HFE-7000 has been reported to break and from new bonds

which results in the development of tribo-films [36]. In addition, C–H bond is weaker than C–F [23,36,41] bonds and C–O bond is weaker than the C–C bond [36,42,43]. Breaking of the molecular structure of the refrigerant means it could result in the generation of carbonyl products e.g. esters which are also polar in nature [44]. On the other hand electron mobility in Graphene is extremely high [45] and graphene crystallites demonstrate graphene to have the fastest electron motilities in comparison to all other materials [45]. Graphene also shows exceptional electrocatalytic behaviour that is accredited to its unique chemical and physical properties, such as subtle electronic characteristics (p-p
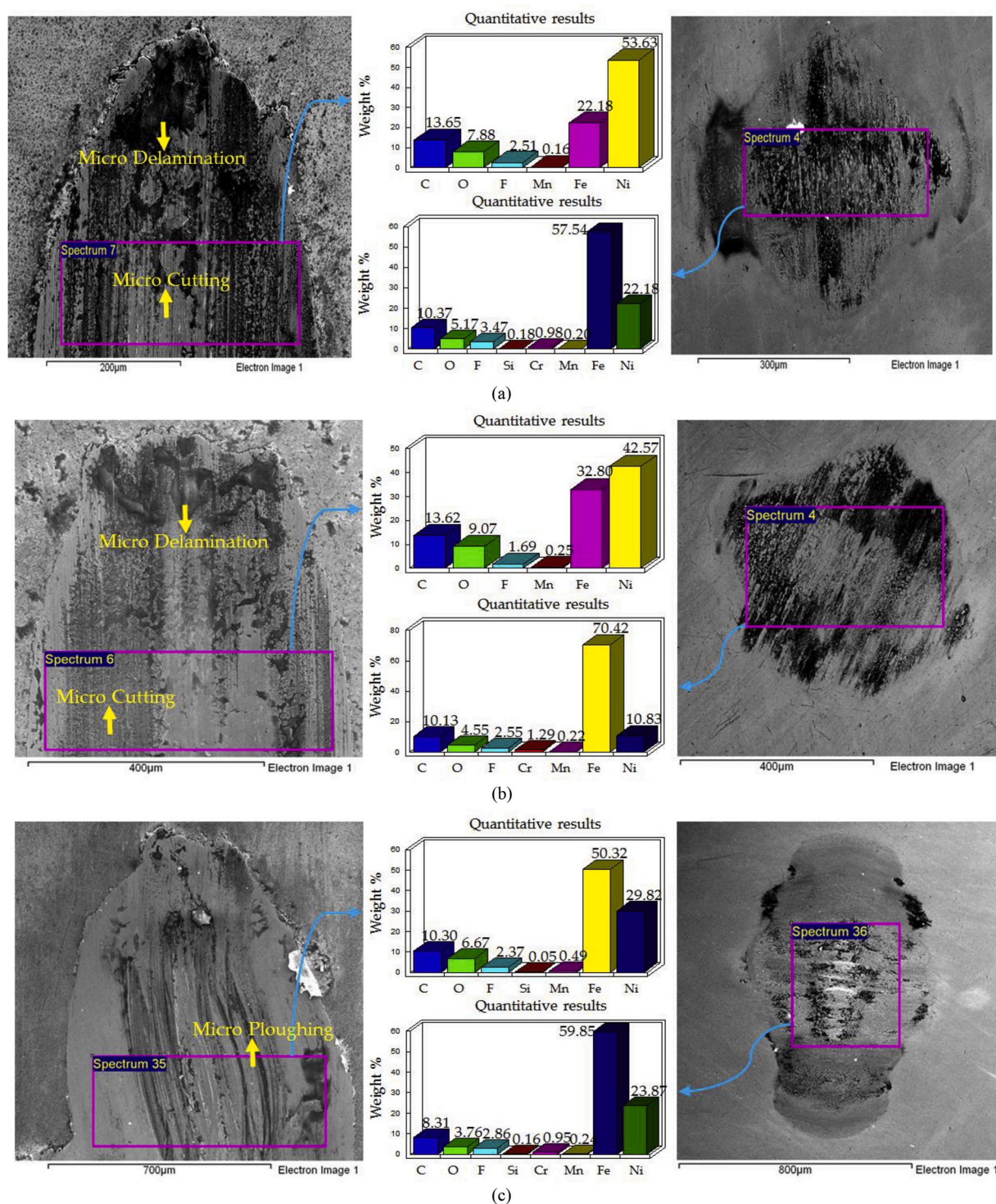
20

Fig. 18. EDS elemental results and SEM Micrographs of Nickel-only coated flat samples and counter steel ball: (a) 40 °C, 10 N (b) 40 °C, 20 N (c) 40 °C, 30 N.

interactions and its strong absorptive capability) [45,46]. Graphene has large surface area, ballistic electron motilities and excellent conductivity [47]. In addition the presence of the extended C=C conjugation in graphene is also likely to shuttle electrons [47]. These properties show that Graphene is not only rich in electrons but also has the fastest electron mobility and possesses electrocatalytic behaviour which results in pulling out of graphene nanoparticles from the nanocoatings due to the polar nature of the refrigerant. Nano particles with larger particle size ($\geq$ 20 nm) were used in all the other coatings prepared in this study except for Graphene for which nanoparticles of 6–8 nm were used. The

small size of the electron rich Graphene nanoparticles in the presence of polar molecules at fully lubricated refrigerant conditions at constant reciprocating motion ejects the nanoparticles from the coatings. In addition, very low oxygen and fluorine was detected on the wear tracks of these tests post experimentation showing that Graphene is not favourable for the generation of tribo-films at low operation temperatures and low applied loads. Increase in load to 30 N at 20 °C facilitates the chemical breakdown of the refrigerant and establishment of tribological films on the wear scar which reduces wear at 20 °C/30 N. Increase in load also helps retain Graphene in the Nickel matrix which
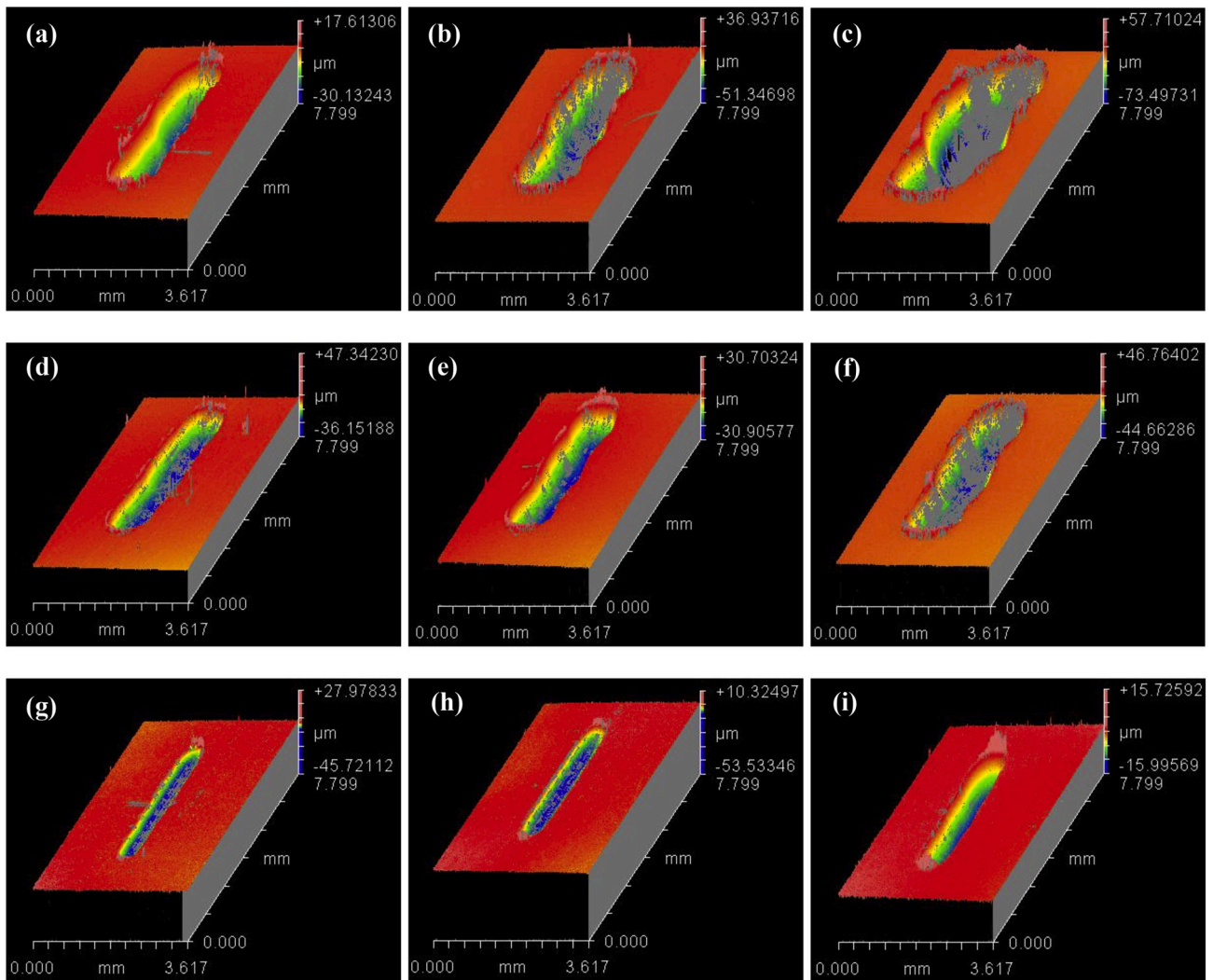
Fig. 19. 3D plots of the wear tracks of Ni–ZrO$_2$ coated specimens. (a) 20 °C, 10 N (b) 20 °C, 20 N (c) 20 °C, 30 N (d) 30 °C, 10 N (e) 30 °C, 20 N (f) 30 °C, 30 N (g) 40 °C, 10 N (h) 40 °C, 20 N (i) 40 °C, 30 N.
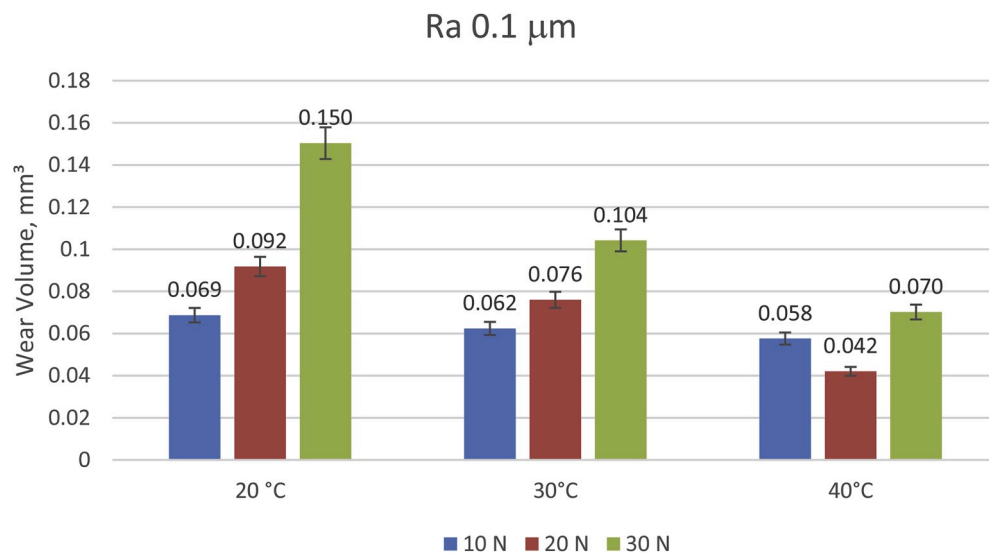

Fig. 20. Wear volume plot of uncoated disc sample with R$_a$ 0.1 μm [36].
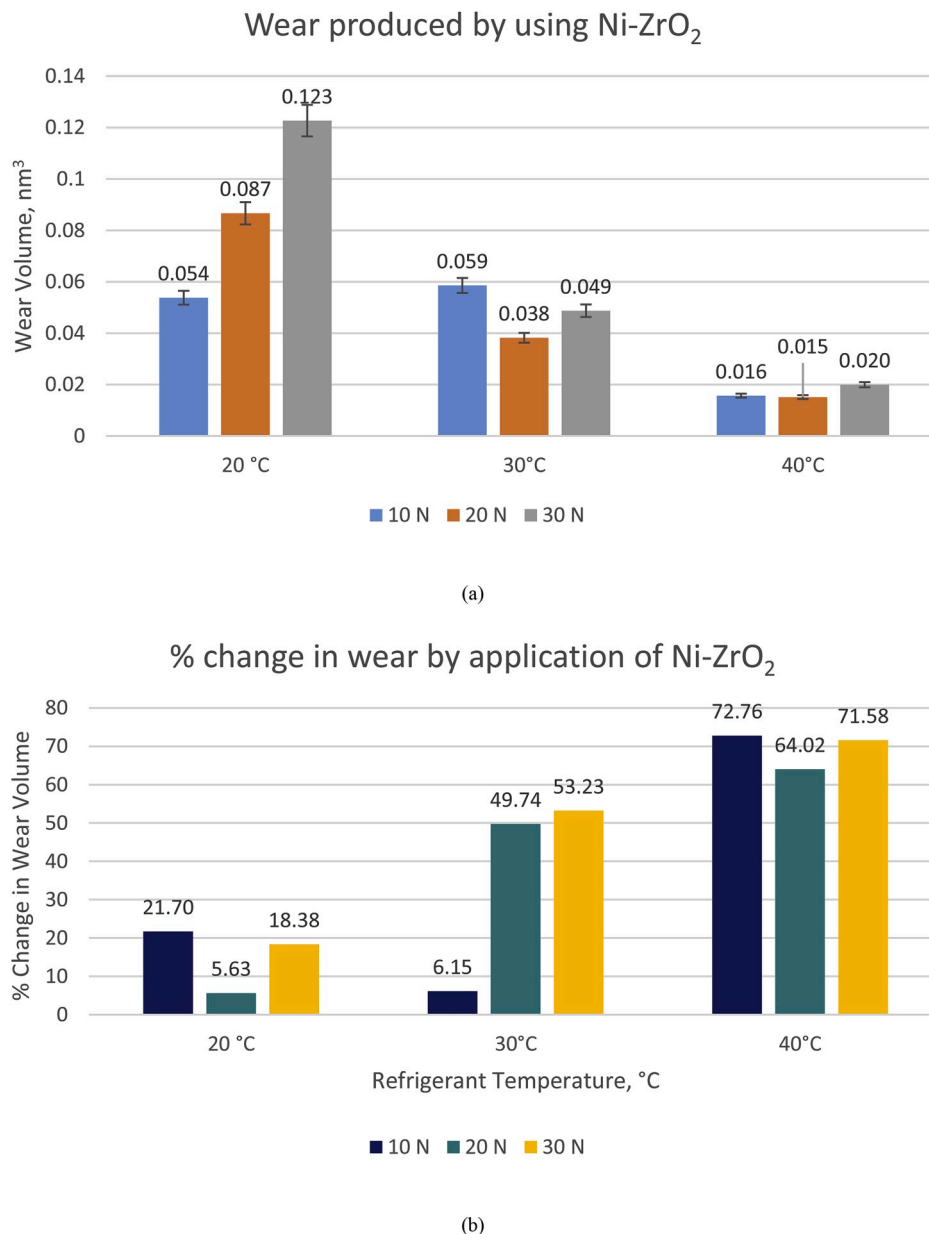
Wear produced by using Ni-ZrO$_2$

(a)

% change in wear by application of Ni-ZrO$_2$

(b)

Fig. 21. (a) Wear volume plot of Ni–ZrO$_2$ (b) Change in wear volume by application of Ni–ZrO$_2$.

helps in wear reduction.

Increasing the refrigerant temperature to 30 °C had a slight positive effect on wear at 10 N load and 30 N load. Higher percentage of Nickel is also observed on the wear track as shown in Fig. 14 confirming a decrease in wear. EDS results also show a greater presence of oxygen and fluorine signifying a higher presence of surface tribo-films as compared to the tests conducted at 20 °C. Increasing the temperature of the refrigerant to 30 °C at 20 N load however did not have a positive impact on wear and wear volume in fact increased at these conditions, this is probably due to the accelerated development of tribo-films on the un-coated surface as compared to Ni-GPL coated surface under these testing conditions. Increasing the refrigerant temperature further to 40 °C resulted in a drop in wear at all loads, highest drop in wear was observed at 10 N load and the least positive effect on wear was seen at 20 N load. EDS results presented in Fig. 15 reveal the highest percentage of Nickel presence at 40 °C/10 N for Ni-GPL amongst all the tests and a good percentage of oxygen/fluorine presence which help reduce wear. Unlike Ni–SiC, Ni–ZrO$_2$ and the uncoated steel, minimum wear for Ni-GPL coatings was also observed at 40 °C/10 N.

Results of wear for Nickel-only coatings have been presented in Fig. 25. The results of wear volume show a different trend at 20 °C refrigerant temperature as compared to uncoated, Ni–ZrO$_2$, Ni–SiC and Ni–Al$_2$O$_3$ coated contacts; at 20 °C all these samples showed an increase in wear whereas Nickel-only coatings show a decrease in wear by increasing the load at 20 °C refrigerant temperature. For Nickel-only coatings a combination of micro-delamination and micro-cutting is observed at 20 °C/10 N; the wear mechanism however shifts mainly towards micro-cutting and less micro-delamination occurs with increase in applied load as shown in Fig. 16, this shift in wear mechanism helps reduce wear with increase in load for Nickel-only coatings at 20 °C refrigerant temperature. Comparison of the wear volume between un-coated and Nickel coated samples show a decline in wear volume by the application of Nickel-only coatings. Increasing the load at 20 °C pro-duces a greater percentage reduction in wear, this is due to fact that wear reduces with increase in load for Nickel-only coatings at 20 °C. By increasing the refrigerant temperature to 30 °C a reduction in wear is observed. Maximum wear at 30 °C refrigerant temperature is observed at 20 N load which is due to the accelerated micro-cutting of the coating
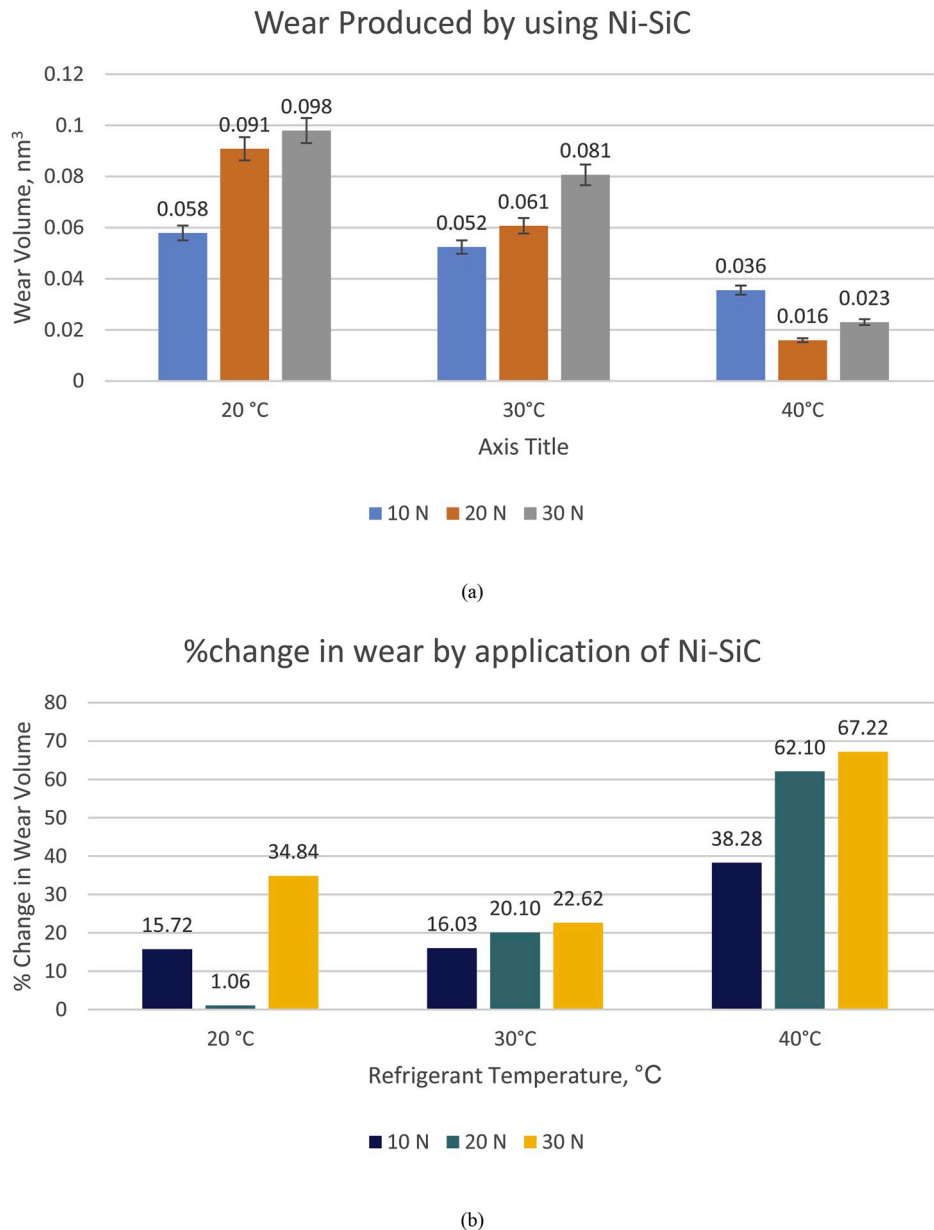
Wear Produced by using Ni-SiC

(a)

%change in wear by application of Ni-SiC

(b)

Fig. 22. (a) Wear volume plot of Ni–SiC (b) Change in wear volume by application of Ni–SiC.

at 30 °C/20 N in comparison to 30 °C/10 N and 30 °C/30 N as shown in Fig. 17. EDS results also confirm a lesser presence of Nickel at 30 °C/20 N in contrast to 30 °C/10 N and 30 °C/30 N. Percentage effect on wear volume by applying Nickel-only coatings shows a decrease in wear at all applied loads in comparison to uncoated steel sample. A further rise in the temperature of the refrigerant to 40 °C decreases wear. Similar to Ni-GPL; wear increase with increase in load at 40 °C and also the least amount of wear is produced at 40 °C/10 N. Comparing to the uncoated steel, wear has reduced by applying Nickel-only coatings. Maximum positive effect on wear occurs at 40 °C/10 N. Due to an increase in wear volume with increase in load at 40 °C, the positive effect on wear drops from about 85% to about 49%.

To summarize, similar to the behaviour noted by using uncoated steel wear volume also decreased with increase in refrigerant temperature for *all* of the coatings used in this study. Wear primarily occurred due to micro-delamination, micro-cutting and micro-ploughing. Wear mechanism depends on the type of coating [32,34], wear phenomenon also shifted from one to another for the same coatings at different testing conditions. The amount of wear volume produced is also dependent on

the production of protective surface tribological films on the mating metals, increasing the temperature of the refrigerant increases the reactivity of the refrigerant HFE-7000 with the rubbing surfaces which accelerates the formation of these tribological films on the mating surfaces which help reduce wear [24,36]. Irrespective of the coatings tested in this study when the amount of fluorine and/or oxygen detected on the rubbing surfaces increased with an increase in refrigerant temperature indicates a higher presence of tribological films on the top surfaces of the interacting parts which play a vital role in wear reduction. Micro-hardness and hardness to elastic modulus ratio (H/E) improved by applying Nickel based coatings on the steel substrate. Ni-GPL showed the highest hardness values followed by Ni–Al_2O_3. Ni–Al_2O_3 displayed the highest hardness to elastic modulus (H/E) ratio, the second best (H/E) ratio was shown by Ni-GPL. Ni–ZrO_2 showed an improvement in wear at all operating conditions in comparison to the uncoated steel and the highest drop in wear was observed at higher refrigerant temperature of 40 °C at which wear dropped by more than 72% at 40 °C/10 N. Ni–SiC coatings also had a positive effect on wear reduction, similar to Ni–ZrO_2, Ni–SiC coatings also showed good wear performance for all testing
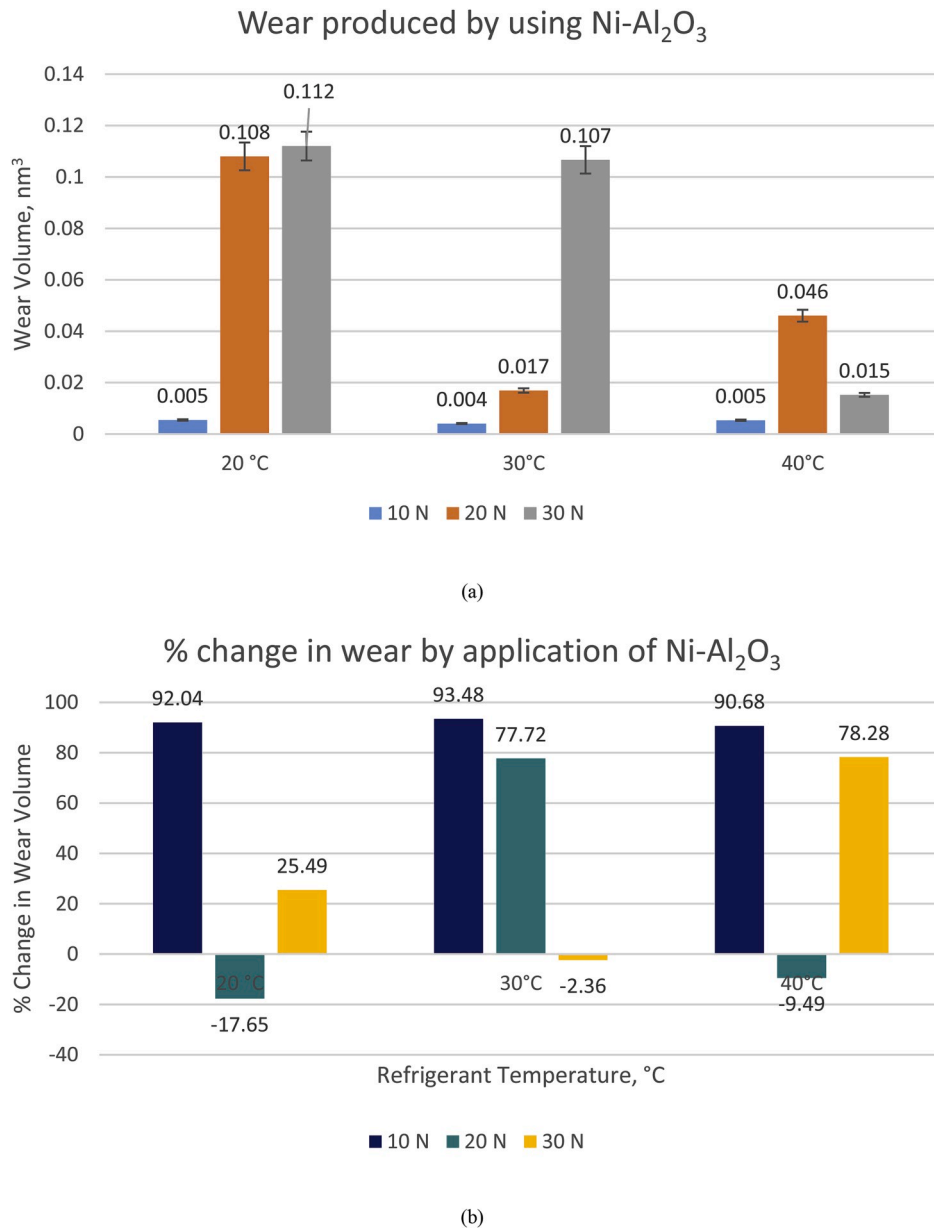
(a)

(b)

Fig. 23. (a) Wear volume plot of Ni–Al$_2$O$_3$ (b) Change in wear volume by application of Ni–Al$_2$O$_3$.

conditions and maximum positive effect on wear was also observed at 40 °C refrigerant temperature. However the maximum effect on wear loss occurred at 40 °C/30 N by using Ni–SiC coatings whereas the maximum effect on wear loss for Ni–ZrO$_2$ was at 40 °C/10 N. Ni–Al$_2$O$_3$ coatings gave some interesting results in terms of wear volume. In comparison to the uncoated steel samples, three of the testing conditions (20 °C/20 N, 30 °C/30 N and 40 °C/20 N) resulted in an increase in wear volume by employing Ni–Al$_2$O$_3$ coatings. Ni–Al$_2$O$_3$ coatings are prone to delaminate under the influence of reciprocating motion [24,34] which increases wear. Ni–Al$_2$O$_3$ coatings however presented the second best hardness and the best (H/E) ratio amongst all the coatings produced which results in a significant drop in wear loss especially at low loads; all the test conducted at low loads (20 °C/10 N, 30 °C/10 N and 40 °C/10 N) show a drop in wear by more than 90%. None of the other coatings tested in this study show such a significant drop in wear at low loads; 20 °C/30 N, 30 °C/20 N and 40 °C/30 N also proved to be beneficial in wear reduction. Ni-GPL displayed the best micro-hardness value but resulted in a drastic increase in wear volume at low testing temperature of 20 °C and at low loads. This is believed to be due to the incompatibility of

HFE-7000 with Graphene nanoparticles and the slower formation of tribo-films. Increasing the load and the temperature of the refrigerant however proves to be beneficial in reducing wear for Ni-GPL, wear drops at higher temperature and at higher loads due to the acceleration in the production of tribo-films which help decrease wear. All the tests conducted at 40 °C for Ni-GPL show a reduction in wear volume. Nickel-only coatings also provided good results in terms of wear reduction. Higher wear reduction was noted at higher refrigerant temperatures. Nickel-only coatings also produced the maximum drop in wear at 40 °C/10 N. When comparing to uncoated steel, Nickel-only coatings proved to be beneficial in reducing wear at all the testing conditions. Good performance of Nickel-only coatings in comparison to other coatings is believed to be associated with three body abrasive wear. The wear debris produced during testing have been reported to be entrapped in the disc and refrigerant holding cup [36]; all of the nanocomposite coatings contain hard nanoparticles, the worn out coating and hard nanoparticles trapped in the cup cause three body wear and result in increase in wear. Wear debris produced by Nickel-only coatings do not contain hard nanoparticles and three body abrasive
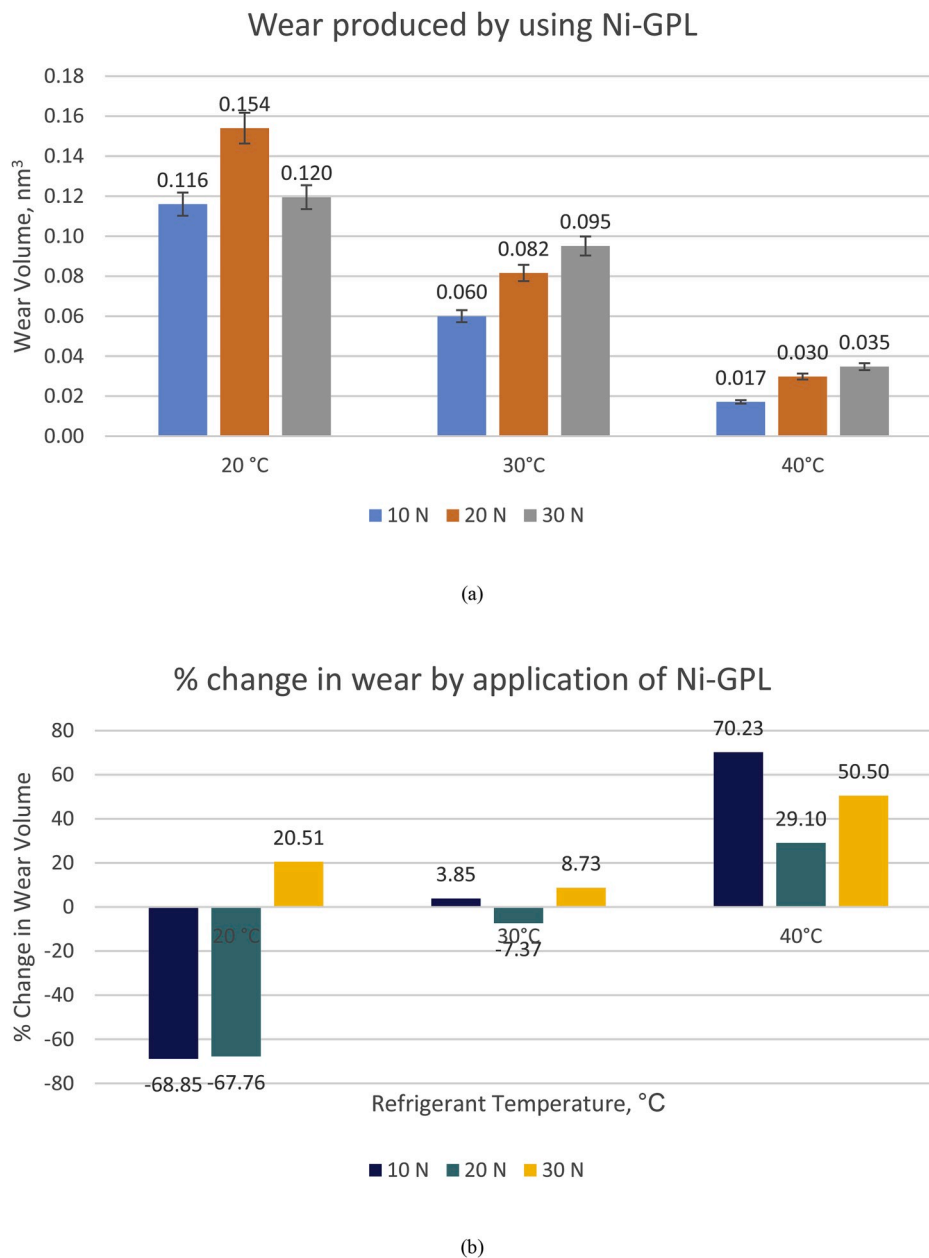
Wear produced by using Ni-GPL

(a)

% change in wear by application of Ni-GPL

(b)

Fig. 24. (a) Wear volume plot of Ni-GPL (b) Change in wear volume by application of Ni-GPL.

wear phenomenon which is also believed to take place when using Nickel-only coatings does not produce the same amount of damage. Nickel-only coatings are also believed to be more beneficial in the development of surface films in comparison to the coatings which have different nano-particles in the Nickel matrix.

6. Friction

The influence on the friction coefficient by the application of coatings was also analysed in this study. Results of the coefficient of friction have been presented as real-time friction coefficient graphs and also as average coefficient of friction plots. Results obtained from each of the coatings were also compared to the uncoated samples with R_a of 0.1 μm. Results of the average friction coefficient of the uncoated samples have been provided in Fig. 26 for reference.

Results of Ni–ZrO$_2$ coated steel have presented in Fig. 27. Fig. 27 (a) and 27 (b) and 27 (c) show the real-time coefficient of friction plots. All these plots show a decrease in the friction coefficient values with

increase in applied load. An increase in the temperature of the refrigerant from 20 °C to 30 °C does not a have noticeable change on the friction coefficient values. Increasing the temperature of the refrigerant to 40 °C however has a positive influence on the friction coefficient values. The friction coefficient drops at each of the applied normal loads by increasing the refrigerant temperature from 20 °C to 40 °C, this is also evident from the average coefficient of friction plots shown in Fig. 27 (d). There are more fluctuations in the friction coefficient at lower loads, increase in load at any given temperature reduces not only the coefficient of friction but also the fluctuations in the friction coefficient.

This decline in friction coefficient with increase in refrigerant temperatures and the decrease in average friction coefficient values with increase in normal load at any given temperature is linked with the development of protective tribological films on the surfaces of the interacting parts. A comparison of the average coefficient of friction of Ni–ZrO$_2$ to uncoated steel is shown in Fig. 27 (e). The plot shows that all operating conditions are not beneficial in reducing friction, a slight increase in the average coefficient of friction is observed at 20 °C/20 N and
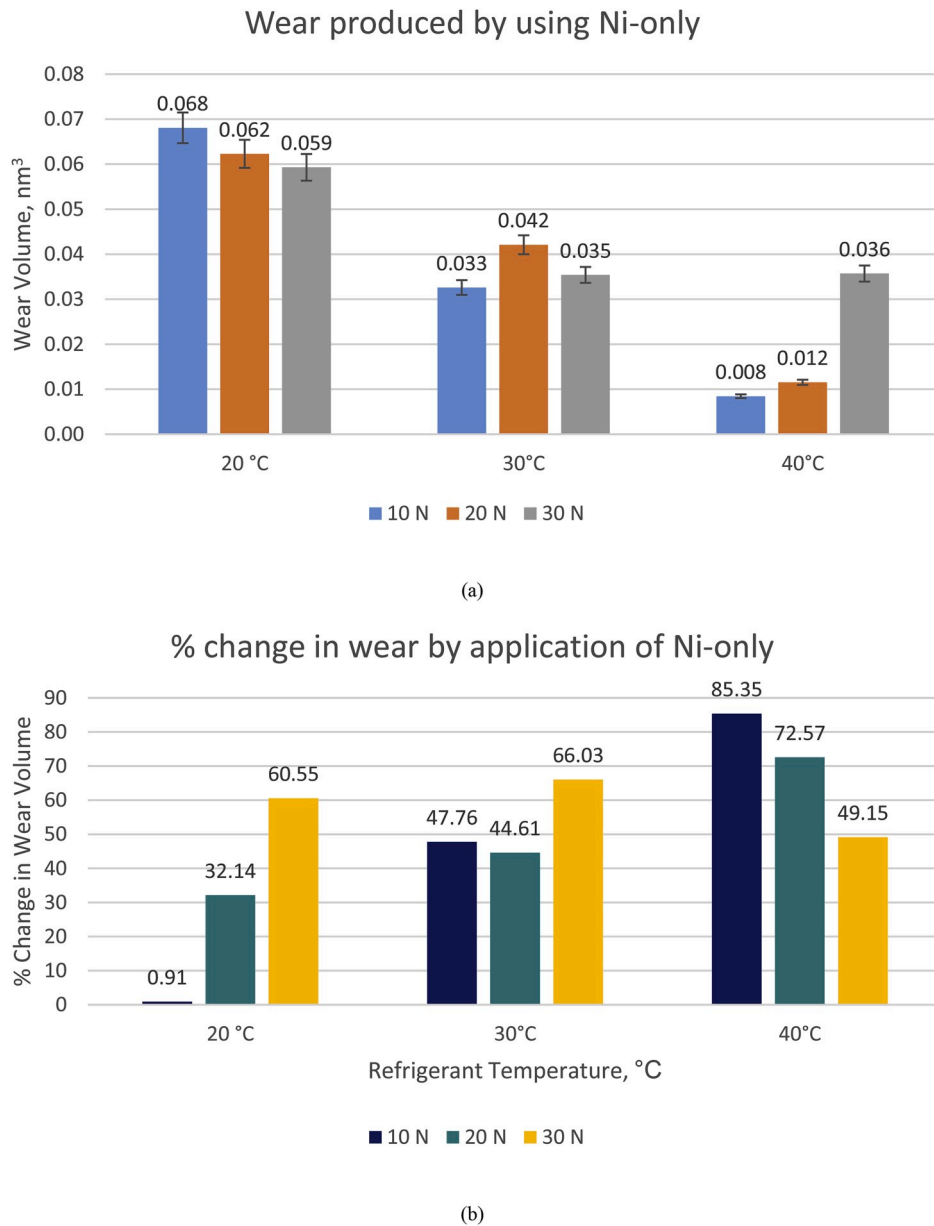
Wear produced by using Ni-only

(a)

% change in wear by application of Ni-only

(b)

Fig. 25. (a) Wear volume plot of Nickel (b) Change in wear volume by application of Nickel.

30 °C/10 N. These two testing conditions also proved to be beneficial in improving wear. Maximum improvement in friction coefficient was observed at 20 °C/10 N. 40 °C refrigerant temperature improved friction at all loads when compared to the uncoated steel samples.

Fig. 28 shows the results of the coefficient of friction obtained by applying Ni–SiC coatings. Similar to Ni–ZrO$_2$ nanocomposite coatings, Ni–SiC coatings also show a drop in the friction coefficient with increase in applied normal load at any given temperature. In addition a constant decline in the coefficient of friction is observed with an increase in refrigerant temperature. The average coefficient of friction decreases by increasing the load at all testing temperatures and a decline in the average coefficient of friction by increasing the refrigerant temperature to 40 °C from 20 °C can be observed in Fig. 28 (d). Similar to the real time coefficient of friction results, higher fluctuations in the friction coefficient are visible at lower loads and increase in load reduces the fluctuations in the friction coefficient.

Comparing the results of the average friction coefficient of Ni–SiC to the uncoated steel shows an improvement in the friction coefficient at almost all of the testing conditions, only 20 °C/30 N and 40 °C/10 N

showed a slight increase (less than 1%) in the average friction coefficient by applying Ni–SiC coatings. Other than these two conditions an improvement in the average coefficient can be clearly seen in the plot presented in Fig. 28 (e). Testing conditions of 30 °C/20 N showed the maximum improvement in the coefficient of friction by applying Ni–SiC coatings.

Results of the coefficient of friction for Ni–Al$_2$O$_3$ have been presented in Fig. 29. These results show a different behaviour in comparison to Ni–ZrO$_2$ and Ni–SiC.

Fluctuations and spikes in the real-time coefficient of friction graphs at 10 N load as observed for the previous two coatings were not observed in the case of Ni–Al$_2$O$_3$. At low loads Ni–Al$_2$O$_3$ also presented the best wear results compared to all the other coatings tested in this study. A reduction in wear at low loads leads to less wear debris and a significant reduction in three-body abrasive wear which reduces the variations/ fluctuations in the coefficient of friction. Ni–Al$_2$O$_3$ nanocomposite coatings had the best surface finish amongst all the coatings prepared in this study and had R$_a$ of only 0.045 µm. A smoother surface means less asperity interactions which reduces friction as well as wear. Average
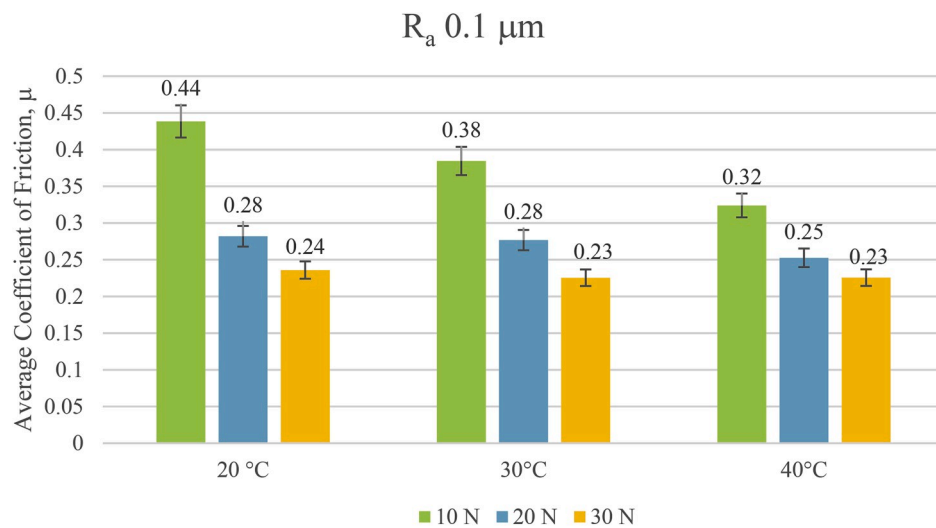
R_a 0.1 μm

Fig. 26. Average coefficient of friction plot for uncoated steel sample with R_a 0.1 μm [36].

Fig. 27. Coefficient of friction graphs for Ni–ZrO$_2$: Real-time coefficient of friction at refrigerant temperature (a) 20 °C (b) 30 °C (c) 40 °C (d) Average coefficient of friction plot (e) Percentage in average friction coefficient by applying Ni–ZrO$_2$.
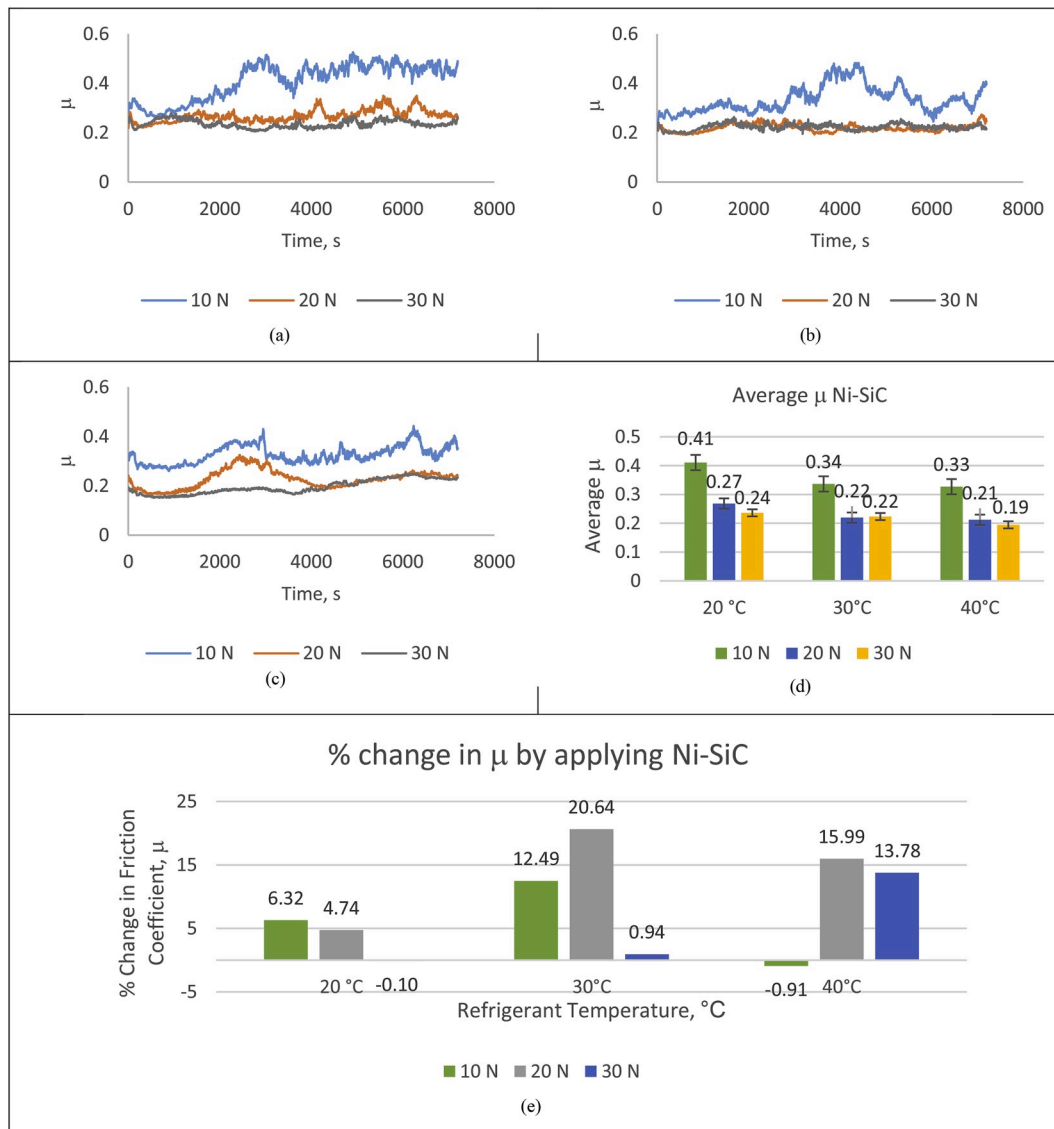
Fig. 28. Coefficient of friction graphs for Ni–SiC: Real-time coefficient of friction at refrigerant temperature (a) 20 °C (b) 30 °C (c) 40 °C (d) Average coefficient of friction plot (e) Percentage in average friction coefficient by applying Ni–SiC.

friction coefficient plots for Ni–Al₂O₃ are also different from the Ni–SiC, Ni–ZrO₂ and the uncoated steel samples. Increasing the load to 20 N from 10 N at 20 °C reduces friction coefficient, but a further increase in load to 30 N does not affect the average coefficient of friction. Increasing the temperature to 30 °C does result in a drop in the friction coefficient compared the 20 °C, however increasing load at 30 °C does not have any influence on the coefficient of friction. Increasing the temperature to 40 °C increases the friction coefficient slightly at 40 °C/10 N in comparison to 30 °C/10 N. 40 °C/20 N and 40 °C/30 N show a drop in the average friction coefficient compared to 30 °C/20 N and 30 °C/30 N. Comparing the average coefficient of friction results of Ni–Al₂O₃ to uncoated steel show an improvement in the coefficient of friction values at all the testing conditions. The highest improvement was noted at 30 °C/10 N at which the coefficient of friction improved by over 40%, 30 °C/10 N also showed the best improvement in wear for Ni–Al₂O₃. Ni–Al₂O₃ also did not show an increase in the average friction coefficient values in comparison to uncoated steel at any of the testing conditions.

Similar to the results of wear, Ni–GPL also showed poor coefficient of friction results at lower refrigerant temperature. At 20 °C an increase in applied load to 20 N from 10 N dropped the coefficient of friction but an additional increase in load to 30 N from 20 N at 20 °C did not affect the

average coefficient of friction as shown in Fig. 30. Ni-GPL coatings had the highest average surface roughness value (1.17 μm) compared to all the other coatings and also when compared to the uncoated steel disc samples. This high surface value was due the presence of nano graphene particles at the very top of the surface and also due to particle agglomeration. 20 °C/10 N showed an improvement in the coefficient of friction when compared to the uncoated steel, however increase in load at 20 °C produced larger coefficient of friction values in comparison to uncoated steel and the friction coefficient increased by approximately 45% at 20 °C/30 N. Increase in refrigerant temperature to 30 °C from 20 °C however proved to be extremely beneficial in reducing the coefficient of friction and when compared to the uncoated steel, the coefficient of friction dropped by more than 33% at 30 °C/10 N. Although the refrigerants viscosity decreases with an increase in temperature which leads to more asperity interaction that should increase friction, but the friction coefficient reduces which is because of the increase in refrigerants reactivity with the rubbing surfaces and formation of tribofilms. Wear however did not show a very significant improvement for 30 °C tests and in fact wear volume increased at 30 °C/20 N. Increasing the temperature of the refrigerant to 40 °C drops the coefficient of friction at 40 °C/20 N and 40 °C/30 N in comparison to the tests
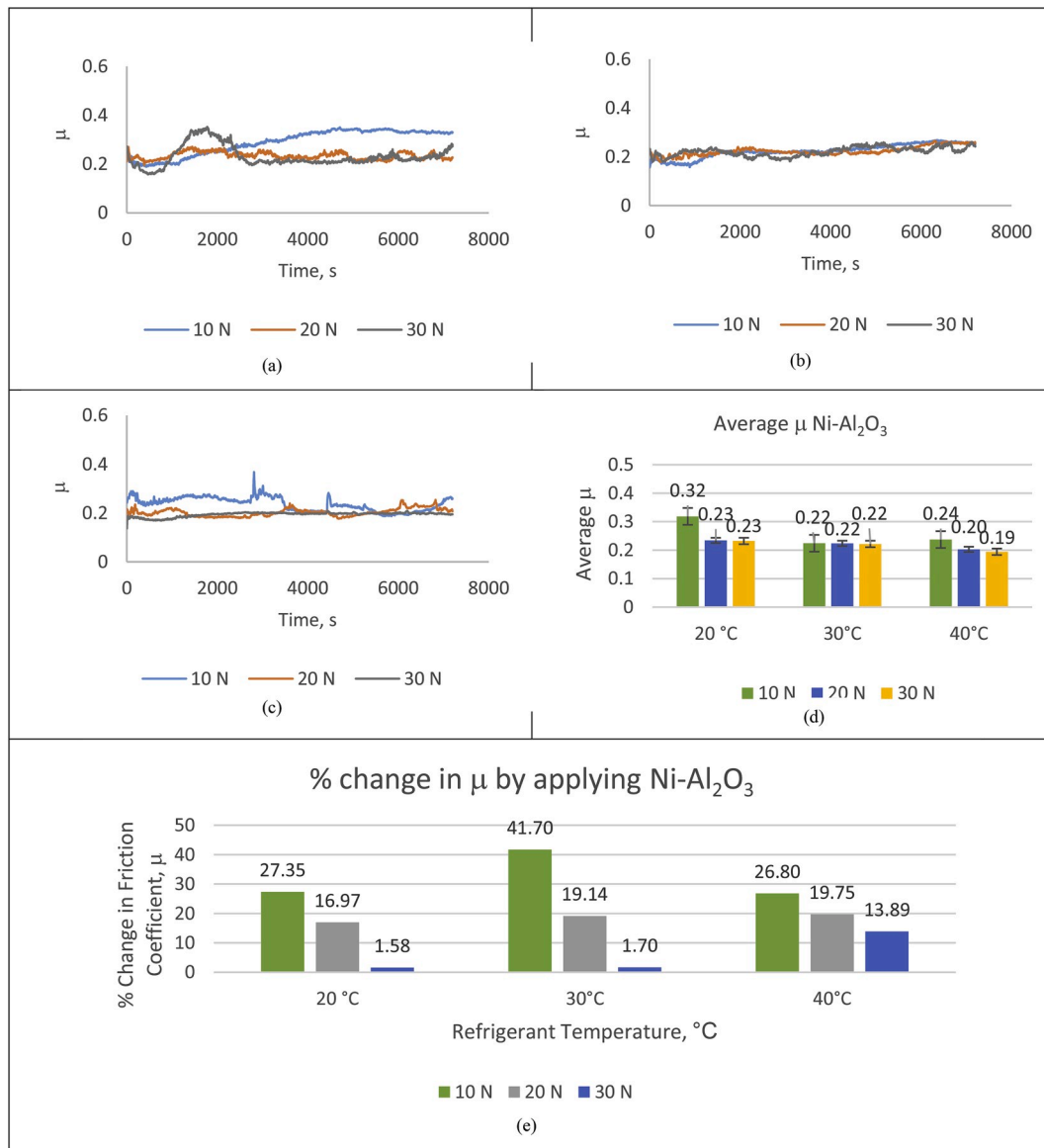
Fig. 29. Coefficient of friction graphs for Ni–Al$_2$O$_3$: Real-time coefficient of friction at refrigerant temperature (a) 20 °C (b) 30 °C (c) 40 °C (d) Average coefficient of friction plot (e) Percentage in average friction coefficient by applying Ni–Al$_2$O$_3$.

conducted at lower temperatures, however in contrast to 30 °C/10 N the average friction coefficient is seen to increase slightly at 40 °C/10 N. Comparing the results of Ni-GPL to uncoated steel also show that these coatings improve friction at 40 °C at all the loads. Wear was seen to improve as well at 40 °C for Ni-GPL.

Results obtained by the application of Nickel-only coatings have been presented in Fig. 31. The results of the real-time friction coefficient show variations in the coefficient of friction as well especially at low loads. Increasing the load at any particular temperature also reduces the real-time coefficient of friction as well as the average friction coefficient. Increase in temperature of the refrigerant from 20 °C to 30 °C did not have any influence on the average friction coefficient. An additional rise in the temperature of the refrigerant to 40 °C however produces a drop in the coefficient of friction values. 40 °C/30 N presented the least average friction coefficient not only for the Nickel coatings but also in comparison to all the other coatings. Nickel-only coatings also had the second best surface finish amongst all the coatings. When comparing the data of the average friction coefficient to the uncoated steel a very slight increase in the friction coefficient was observed at 20 °C/30 N and an increase in friction was also observed at 30 °C/30 N. Other than these

two conditions the friction coefficient improved by applying Nickel-only coatings.

Wear and friction coefficient for Nickel-only coatings did not follow the same trend. At 20 °C and 40 °C wear increases by increasing the load whereas friction coefficient decreases by increasing the applied load at 20 °C and 40 °C for Nickel-only coatings. For 20 °C, parentage change in coefficient of friction drops by increasing the load whereas for 20 °C, percentage change in wear increases by increasing the load. At 40 °C, percentage change in wear volume decreases with increase in load while percentage change in the friction coefficient increases by increasing the load. Wear volume results improved at all the testing conditions by applying Nickel-only coatings whereas two of the testing conditions increased friction coefficient for Nickel-only coatings.

An improvement in the coefficient of friction was observed by the deposition of nanocomposite coatings for most of the conditions. Cavities and micro-dimpled groves have been known to enhance the tribological behaviour and performance of rubbing parts [48,49] and pores in Ni–Al$_2$O$_3$ coatings have been reported to retain liquid refrigerant and to improve the lubricity of interacting parts which helps improve wear [24]. All the prepared coatings have micro-pores as shown in Fig. 1,
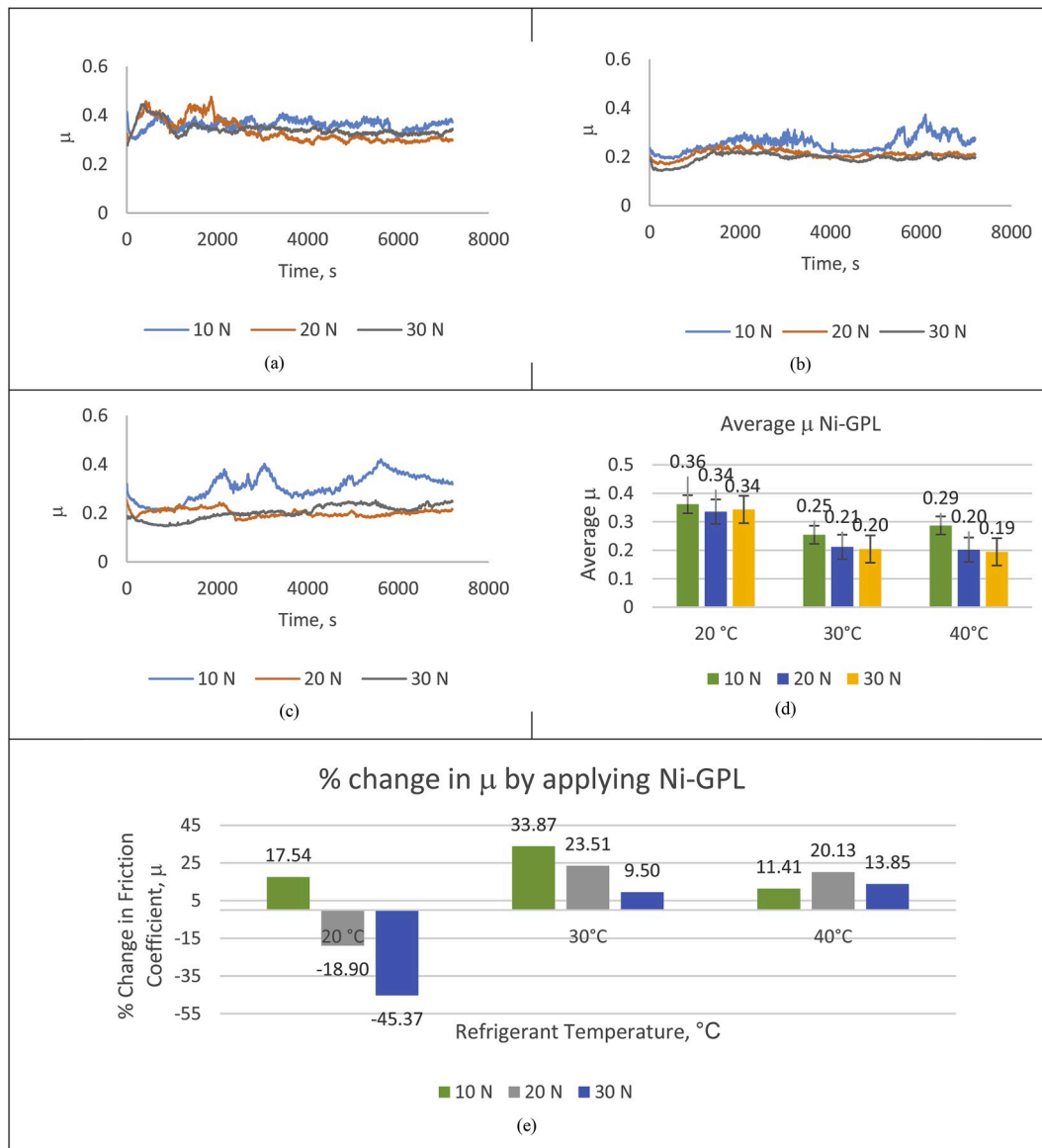
Fig. 30. Coefficient of friction graphs for Ni-GPL: Real-time coefficient of friction at refrigerant temperature (a) 20 °C (b) 30 °C (c) 40 °C (d) Average coefficient of friction plot (e) Percentage in average friction coefficient by applying Ni-GPL.

these micro-pores also help in lubricant retention which reduces friction. The peaks in the real-time coefficient of friction appear due to the variation in the contact area of the counter steel ball. Wear occurs on the steel ball which increases the apparent contact area during the course of a test. The increase in contact area increases the coefficient of friction. The Hertzian diameter of 52100 steel ball is known to increase with increase in wear for a reciprocating/oscillating ball-on-flat contact geometry [50]. The wear scar produced on a 52100 steel ball with a fixed steel ball against a reciprocating disc in a ball-on-flat contact geometry has also been reported to change shape which increases the apparent area of contact and reduces contact pressure [51]. High magnification SEM images of the wear scar generated on the steel ball show that the shape and size of the wear scar changes with a change in loading conditions and by changing the type of coating. Wear scar on a stationary 52100 steel ball loaded against a reciprocating flat sample shifts from circular contact at lower loads to an elliptical contact at higher applied loads [36,51]. Multiple peaks and sharp gradients were generated at a few of the testing conditions as seen in some of the real-time coefficient of friction graphs. The first peak is due to the initiation of the change in the apparent contact area of the steel ball and the additional peaks

indicates a further alteration in the contact area of the ball [36]. Fluctuations and variations in the friction coefficient are believed to be due to the alteration in the area of contact of the steel ball, due to three body abrasive wear caused by the wear debris trapped inside the refrigerant holding cup, due to the uneven formation of surface tribo-films especially at lower loads and due to the adhesion of the worn coatings on the surface of the steel ball; continuous reciprocating motion of the steel ball with adhered particles leads to rise in fluctuations in the friction coefficient.

Formation of oxygen and fluorine containing tribo-films on the mating surfaces by different refrigerants has been known to enhance the tribological i.e. wear, lubricity and friction performance of mating machine parts [7,23,24,52–58]. EDS analysis was performed within the contact region on each and every sample pair tested in this study. EDS results show a clear presence of oxygen and fluorine post experimentation. Pre-test EDS elemental analysis was also done on each of the prepared coatings and also on the steel balls, the results did not show any fluorine. The test chamber was vacuumed before starting any test which leads to the conclusion that the source of fluorine on the surfaces is the refrigerant. Our previous study on uncoated steel contacts showed
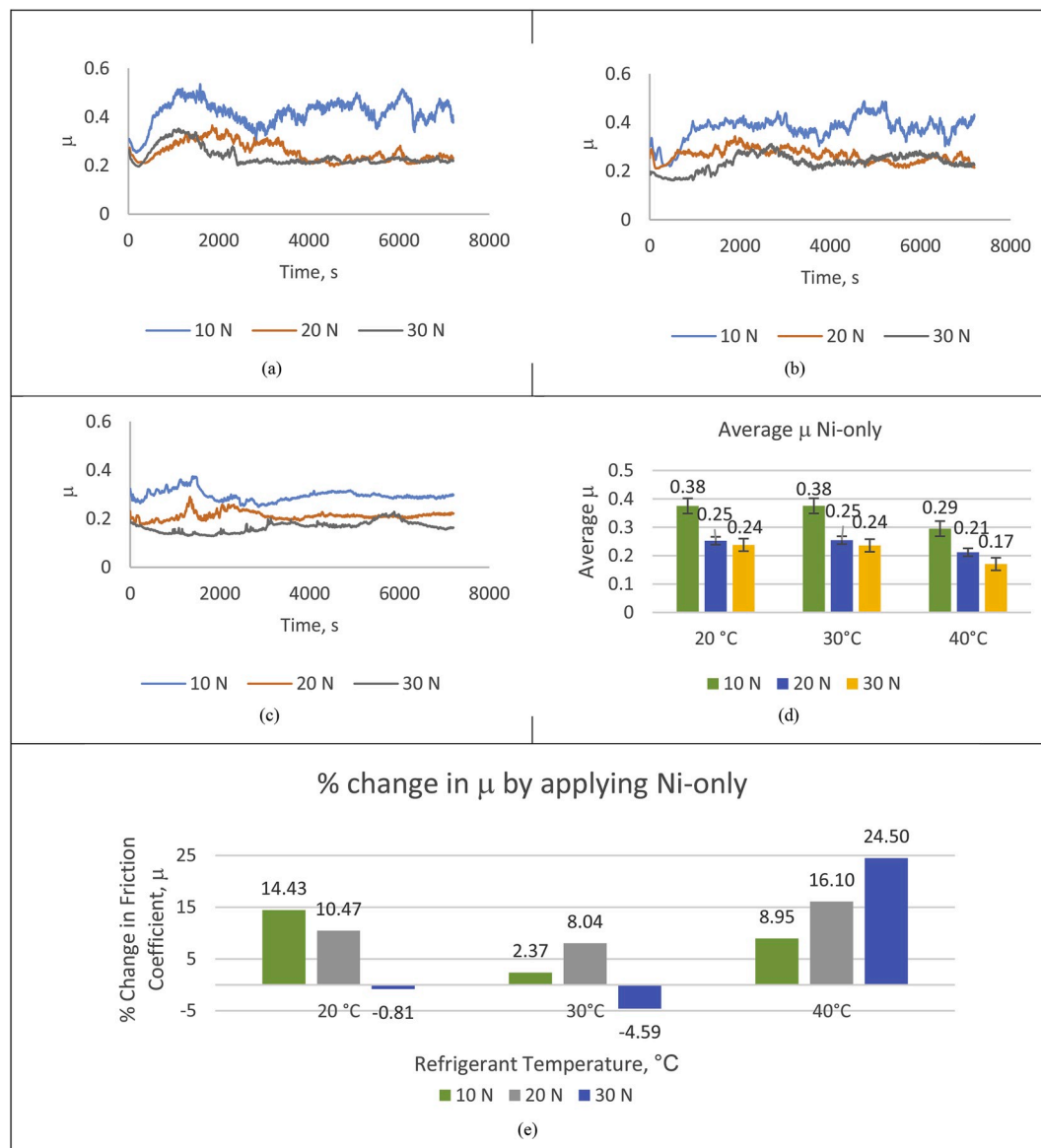
Fig. 31. Coefficient of friction graphs for Nickel-only: Real-time coefficient of friction at refrigerant temperature (a) 20 °C (b) 30 °C (c) 40 °C (d) Average coefficient of friction plot (e) Percentage in average friction coefficient by applying Nickel-only.

that the refrigerant HFE-7000 breaks down by the application of reciprocating motion, load, frictional force and heat [36]. The refrigerant then chemically reacts with the dangling bonds on the freshly exposed metallic surfaces of the steel samples leading to the production of tribo-films [36]. Similar to the uncoated steel discs, HFE-7000 reacted with the coated specimens as F and O were detected at different regions on the wear scar and also on the ball samples. The results also show a decline in friction coefficient and wear for the same applied load at higher refrigerant temperatures. This decrease in wear and friction is because of the increase in reactivity of HFE-7000 with increase in temperature as more oxygen and fluorine was detected at elevated refrigerant temperatures.

7. Conclusions

A modified and commissioned micro-fiction that is fully capable of testing the future generation of environmentally friendly refrigerants was used to assess the performance of Nickel based nanocomposite coatings under HFE-7000 refrigerant by using fully lubricated conditions. Normal load was applied through a stationary steel ball to coated samples under reciprocating motion. The results of friction and wear by using nanocomposite coatings were compared to uncoated contacts in an attempt to enhance the tribological performance of rubbing parts utilizing HFE-7000. Following conclusions can be drawn from this study.

1. Friction and wear of Nickel based coatings applied on a steel substrate under HFE-7000 lubrication is not straightforward. A mix of micro-delamination, micro-cutting and micro-ploughing was observed on the worn surfaces. Wear mechanism was seen to change with a change in coating and also with a change in testing conditions.
2. Deposition of Nickel based coatings on a steel substrate through the pulse coating technique resulted in an improvement in the surface mechanical properties of *all* the prepared coatings. The hardness and the hardness to elastic modulus ratio is improved for all coatings. Ni-GPL nanocomposite coatings showed the highest hardness which was followed by Ni–Al$_2$O$_3$, Ni–SiC, Ni–ZrO$_2$ and Nickel. Nickel-only coatings showed the least values of micro-hardness as it did not contain the hard nanoparticles imbedded in its matrix. Ni–Al$_2$O$_3$ nanocomposite coatings showed the best (H/E) ratio along with the

best surface roughness values while Ni-GPL coatings presented the worst values of surface roughness.

3. Different coatings behaved differently under the same testing conditions.

   a) Ni–Al$_2$O$_3$ nanocomposite coatings showed the best performance in terms of coefficient of friction in comparison to all the other coatings. Testing conditions of 30 °C/10 N showed an improvement of over 40% in the coefficient of friction in comparison to uncoated steel. Wear results showed an improvement of over 90% in wear at low loads by applying Ni–Al$_2$O$_3$ coatings, none of the other coatings showed such an improvement at any of the testing condition. Some of the conditions did result in an increase in wear which is because of the delamination of these coatings. However it can be stated with confidence that Ni–Al$_2$O$_3$ nanocomposite coatings are most suitable for improving both friction and wear at low loads at a range of operating temperatures.

   b) Ni–SiC coatings proved to be beneficial in improving wear in comparison to uncoated steel at all testing conditions. Only a slight improvement of 1% was observed at 20 °C/20 N, other than that all other testing conditions improved wear by at least 15%. Highest improvement was observed at 40 °C/30 N, 40 °C in general proved to be beneficial in improving wear. Friction coefficient also reduced by using Ni–SiC in comparison to uncoated steel at all the testing conditions except for 20 °C/30 N and 40 °C/10 N, these two conditions increased the friction coefficient but only by less than 1%. Maximum reduction in friction coefficient was observed at 30 °C/20 N. This leads to the conclusion that Ni–SiC nanocomposite coatings are beneficial in enhancing the tribological performance of rubbing parts in comparison to uncoated steel.

   c) Ni–ZrO$_2$ coatings displayed the best results of wear at 40 °C refrigerant temperature. None of the other coatings showed such an improvement i.e. an improvement of over 64% at all loads at 40 °C. Maximum improvement in wear was observed at 40 °C/10 N and the results also show an improvement in wear at all testing conditions. The results of friction coefficient however show an increase in friction coefficient by almost 1% at 20 °C/20 N and by about 4% at 30 °C/10 N. All other testing conditions show an improvement in friction coefficient by using Ni–ZrO$_2$ coatings and maximum improvement in friction coefficient was observed at 20 °C/10 N. It can be inferred from these results that Ni–ZrO$_2$ coatings are extremely beneficial in reducing wear in comparison to uncoated steel. These coatings can be used with assurance at higher operating temperatures at which not only a substantial reduction in wear was observed but also higher refrigerant temperature resulted in a drop in friction coefficient.

   d) Ni-GPL nanocomposite coatings showed the worst results in terms of friction and wear at lower refrigerant temperature of 20°. The poor performance of Nickel-Graphene coatings is believed to be due the incompatibility of these coatings with HFE-7000. Graphene has large surface area which is rich in fast moving mobile electrons and HFE-7000 is polar in nature. Higher wear at low loads is believed to be due to the ejection of graphene from the surface by the polar refrigerant. Increase in load helps retain Graphene in the Nickel matrix. An increase in refrigerant temperature proves to be extremely helpful in reducing the coefficient of friction. A decrease in the coefficient of friction almost by 34% can be seen at 30 °C/10 N. 30 °C refrigerant temperature however does not show a substantial improvement in wear and 30 °C/20 N conditions resulted in an increase in wear in comparison to the uncoated steel. Refrigerant temperature of 40 °C however proved to be extremely helpful in not only reducing friction but also in reducing wear. Wear volume dropped by about 70% at 40 °C/10 N and by almost 50% at 40 °C/30 N. From these results it can be seen that one has to be extremely careful in using Ni-GPL nanocomposite coatings in systems utilizing HFE-7000. At higher operating temperatures these coatings can be used but if a system is operating at varying load and changing refrigerant temperatures then Ni-GPL coatings would not be recommended.

   e) Nickel-only coatings resulted in an improvement in the microhardness, (H/E) ratio and average surface roughness in comparison to uncoated steel. This helped improve wear at all the operating conditions. Minimum improvement in wear was noticed at 20 °C/10 N and maximum improvement in wear occurred at 40 °C/10 N. Nickel-only coatings did not contain the hard nanoparticles in the Nickel matrix, these hard nanoparticles are believed to increase wear by three body abrasive wear phenomenon when using nanocomposites. Friction coefficient results show a decrease in the coefficient of friction values at 40 °C for all loads. A slight increase in friction coefficient was however observed at 20 °C/30 N and 30 °C/30 N in comparison to uncoated steel. Nickel-only coatings also show very good results especially for wear improvement and these coatings can be recommended for use in HFE-7000 based systems.

4. Friction and wear of Nickel based coatings under HFE-7000 lubrication is a complex mix of different mechanisms which is not only determined by the type of coating but is also highly dependent on the reaction of the refrigerant with the metallic surfaces. Application of load, heat, friction and mechanical motion results in the breakdown of HFE-7000. HFE-7000 breaks and forms new bonds with the freshly exposed worn surfaces. This results in the formation of oxygenated and fluorinated surface films on the top surfaces. These tribo-films result in a drop in friction and wear.

5. It is believed that the nano-particles embedded in the Nickel matrix hinder the development of anti-wear tribo-films and pure metal surfaces are more favourable in the tribo-chemical reaction between the refrigerant and the mating surfaces

6. A general trend in the reduction in wear with increase in refrigerant temperature and a decrease in friction coefficient with increase in applied normal load and temperature can be observed from the results presented in this study. This is due to the increase in reactivity of HFE-7000 with the interacting metals with increase in temperature and load.

7. Nanocomposite coatings show a clear improvement in friction and wear at most of the testing conditions. Selection of a particular coating depends on load and operating temperature.

Declaration of competing interest

There is no known conflict of interest.

CRediT authorship contribution statement

Muhammad Usman Bhutta: Data curation, Formal analysis, Investigation, Methodology, Validation, Writing - original draft. **Zulfiqar Ahmad Khan:** Conceptualization, Formal analysis, Funding acquisition, Investigation, Methodology, Project administration, Resources, Software, Supervision, Validation, Visualization, Writing - review & editing.

Acknowledgments

References

[1] Calm JM. The next generation of refrigerants – historical review, considerations, and outlook. La prochaine génération de frigorigènes – historique, analyse et perspectives 2008;31. 1123-33.

[2] Bhutta MU, Khan ZA, Garland NP, Ghafoor A. A historical review on the tribological performance of refrigerants used in compressors. Tribol Ind 2018;40: 19–51.

[3] Nations U. Montreal Protocol on Substances that Deplete the ozone layer. Montreal, Canada16 September: United Nations Environment Programme; 1987.

[4] Breidenich C, Magraw D, Rowley A, Rubin JW. The Kyoto protocol to the United Nations framework convention on climate change. Am J Int Law 1998;92:315–31.

[5] Wu X, Cong P, Nanao H, Minami I, Mori S. Tribological behaviors of 52100 steel in carbon dioxide atmosphere. Tribol Lett 2004;17:925–30.

[6] Demas NG, Polycarpou AA. Ultra high pressure tribometer for testing CO_2 refrigerant at chamber pressures up to 2000 psi to simulate compressor conditions. Tribol Trans 2006;49:291–6.

[7] Jeon H-G, Oh S-D, Lee Y-Z. Friction and wear of the lubricated vane and roller materials in a carbon dioxide refrigerant. Wear 2009;267:1252–6.

[8] Nunez EE, Polycarpou AA. Wear study of metallic interfaces for air-conditioning compressors under submerged lubrication in the presence of carbon dioxide. Wear 2015;326–327:28–35.

[9] Nunez EE, Demas NG, Polychronopoulou K, Polycarpou AA. Comparative scuffing performance and chemical analysis of metallic surfaces for air-conditioning compressors in the presence of environmentally friendly CO_2 refrigerant. Wear 2010;268:668–76.

[10] Demas NG, Polycarpou AA. Tribological investigation of cast iron air-conditioning compressor surfaces in CO_2 refrigerant. Tribol Lett 2006;22:271–8.

[11] Garland N, Hadfield M. Environmental implications of hydrocarbon refrigerants applied to the hermetic compressor. Mater Des 2005;26:578–86.

[12] Khan ZA, Hadfield M, Tobe S, Wang Y. Ceramic rolling elements with ring crack defects—a residual stress approach. Mater Sci Eng 2004;404:221–6.

[13] Khan ZA, Hadfield M, Tobe S, Wang Y. Residual stress variations during rolling contact fatigue of refrigerant lubricated silicon nitride bearing elements. Ceram Int 2006;32:751–4.

[14] Khan ZA, Hadfield M. Manufacturing induced residual stress influence on the rolling contact fatigue life performance of lubricated silicon nitride bearing materials. Mater Des 2007;28:2688–93.

[15] Sariibrahimoglu K, Kizil H, Aksit MF, Efeoglu I, Kerpicci H. Effect of R600a on tribological behavior of sintered steel under starved lubrication. Tribol Int 2010; 43:1054–8.

[16] Górny K, Stachowiak A, Tyczewski P, Zwierzycki W. Lubricity evaluation of oil–refrigerant mixtures with R134a and R290. Int J Refrig 2016;69:261–71.

[17] ™ 3M. Novec™ 7000 engineered fluid data sheet. https://multimedia.3m.com /mws/media/121372O/3m-novec-7000-engineered-fluid-tds.pdf3M. [Accessed 17 February 2019].

[18] Helvaci H, Khan ZA. Experimental study of thermodynamic assessment of a small scale solar thermal system. Energy Convers Manag 2016;117:567–76.

[19] Helvaci HU, Khan ZA. Heat transfer and entropy generation analysis of HFE 7000 based nanorefrigerants. Int J Heat Mass Tran 2017;104:318–27.

[20] Helvaci H, Khan Z. Thermodynamic modelling and analysis of a solar organic Rankine cycle employing thermofluids. Energy Convers Manag 2017;138:493–510.

[21] Blaineau B, Dutour S, Callegari T, Lavieille P, Miscevic M, Blanco S, et al. Experimental investigation of a dielectric liquid-vapor interface between two vertical planar electrodes: influence of the DC electric field and temperature. Exp Therm Fluid Sci 2019;105:144–52.

[22] Shin J-H, Rozenfeld T, Shockner T, Kumar Vutha A, Wang Y, Ziskind G, et al. Local heat transfer under an array of micro jet impingement using HFE-7000. Appl Therm Eng 2019;113716.

[23] Akram MW, Polychronopoulou K, Polycarpou AA. Lubricity of environmentally friendly HFO-1234yf refrigerant. Tribol Int 2013;57:92–100.

[24] Bhutta M, Khan Z, Garland N. Wear performance analysis of Ni–Al_2O_3 nanocomposite coatings under nonconventional lubrication. Materials 2018;12:36.

[25] ipcc. The intergovernmental panel on climate change, global warming potential values. https://www.ghgprotocol.org/sites/default/files/ghgp/Global-Warming-Potential-Values%20%28Feb%2016%202016%29_1.pdf. [Accessed 17 February 2019].

[26] Chen L, Wang L, Zeng Z, Xu T. Influence of pulse frequency on the microstructure and wear resistance of electrodeposited Ni–Al_2O_3 composite coatings. Surf Coating Technol 2006;201:599–605.

[27] Chen L, Wang L, Zeng Z, Zhang J. Effect of surfactant on the electrodeposition and wear resistance of Ni–Al_2O_3 composite coatings. Mater Sci Eng 2006;434:319–25.

[28] Zhou Q, He CL, Cai QK. Effect of Al_2O_3 powders on properties of electrodeposited Ni matrix. Adv Mater Res 2009;79–82:631–4.

[29] Saha RK, Khan TI. Effect of applied current on the electrodeposited Ni–Al_2O_3 composite coatings. Surf Coating Technol 2010;205:890–5.

[30] Borkar T, Harimkar SP. Effect of electrodeposition conditions and reinforcement content on microstructure and tribological properties of nickel composite coatings. Surf Coating Technol 2011;205:4124–34.

[31] Bajwa R, Khan Z, Nazir H, Chacko V, Saeed A. Wear and friction properties of electrodeposited Ni-based coatings subject to nano-enhanced lubricant and composite coating. Acta Metall Sin 2016;29:902–10.

[32] Bajwa RS, Khan Z, Bakolas V, Braun W. Water-lubricated Ni-based composite (Nsi–Al_2O_3, Ni–SiC and Ni–ZrO_2) thin film coatings for industrial applications. Acta Metall Sin 2016;29:8–16.

[33] Nazir MH, Khan ZA, Saeed A, Bakolas V, Braun W, Bajwa R, et al. Analyzing and modelling the corrosion behavior of Ni/Al_2O_3, Ni/SiC, Ni/ZrO_2 and Ni/graphene nanocomposite coatings. Materials 2017;10:1225.

[34] Nazir MH, Khan ZA, Saeed A, Bakolas V, Braun W, Bajwa R. Experimental analysis and modelling for reciprocating wear behaviour of nanocomposite coatings. Wear 2018;416–417:89–102.

[35] Kasar AK, Bhutta MU, Khan ZA, Menezes PL. Corrosion performance of nanocomposite coatings in moist SO_2 environment. Int J Adv Manuf Technol 2020; 106(11):4769–76.

[36] Bhutta MU, Khan ZA. Friction and wear performance analysis of hydrofluoroether-7000 refrigerant. Tribol Int 2019;139:36–54.

[37] Bhutta MU, Khan ZA, Garland N. Novel experimental setup to assess surfaces in tribo-contact lubricated by the next generation of environmentally friendly thermofluids. Int J Comput Methods Exp Meas 2019;7:226–35.

[38] Bajwa RS, Khan Z, Bakolas V, Braun W. Effect of bath ionic strength on adhesion and tribological properties of pure nickel and Ni-based nanocomposite coatings. J Adhes Sci Technol 2016;30:653–65.

[39] Algul H, Tokur M, Ozcan S, Uysal M, Cetinkaya T, Akbulut H, et al. The effect of graphene content and sliding speed on the wear mechanism of nickel–graphene nanocomposites. Appl Surf Sci 2015;359:340–8.

[40] Jabbar A, Yasin G, Khan WQ, Anwar MY, Korai RM, Nizam MN, et al. Electrochemical deposition of nickel graphene composite coatings: effect of deposition temperature on its surface morphology and corrosion resistance 2017;7: 31100–9.

[41] Gu G, Wu Z, Zhang Z, Qing F. Tribological properties of fluorine-containing additives of silicone oil. Tribol Int 2009;42:397–402.

[42] Muraki M, Sano T, Dong D. Elastohydrodynamic properties and boundary lubrication performance of polyolester in a hydrofluoroether refrigerant environment. Proc IME J J Eng Tribol 2002;216:19–26.

[43] Lide DR. CRC handbook of chemistry and physics. 73rd edition. Boca Raton, Florida: CRC Press; 1992-1993. p. 9–145.

[44] Tsai W-T. Environmental risk assessment of hydrofluoroethers (HFEs). J Hazard Mater 2005;119:69–78.

[45] Brownson DAC, Banks CE. Graphene electrochemistry: an overview of potential applications. Analyst 2010;135:2768–78.

[46] Kang X, Wang J, Wu H, Liu J, Aksay IA, Lin Y. A graphene-based electrochemical sensor for sensitive detection of paracetamol. Talanta 2010;81:754–9.

[47] Liu C, Alwarappan S, Chen Z, Kong X, Li C-Z. Membraneless enzymatic biofuel cells based on graphene nanosheets. Biosens Bioelectron 2010;25:1829–33.

[48] Abdullah MU, Shah SR, Bhutta MU, Mufti RA, Khurram M, Najeeb MH, et al. Benefits of wonder process craft on engine valve train performance. Proc Inst Mech Eng - Part D J Automob Eng 2018.

[49] Bai L, Meng Y, Khan ZA, Zhang V. The synergetic effects of surface texturing and MoDDP additive applied to ball-on-disk friction subject to both flooded and starved lubrication conditions. Tribol Lett 2017;65:163.

[50] Deshpande P, Minfray C, Dassenoy F, Thiebaut B, Le Mogne T, Vacher B, et al. Tribological behaviour of TiO_2 Atmospheric Plasma Spray (APS) coating under mixed and boundary lubrication conditions in presence of oil containing MoDTC. Tribol Int 2018;118:273–86.

[51] Jean-Fulcrand A, Masen MA, Bremner T, Wong JSS. High temperature tribological properties of polybenzimidazole (PBI). Polymer 2017;128:159–68.

[52] Mizuhara K, Akei M, Matsuzaki T. The friction and wear behavior in controlled alternative refrigerant atmosphere. Tribol Trans 1994;37:120–8.

[53] Kawahara K, Mishina S, Kamino A, Ochiai K, Okawa T, Fujimoto S. Tribological evaluation of rotary compressor with HFC refrigerants. In: International compressor engineering conference purdue university, Indiana, USA, 23-26 july; 1996. Paper 1141.

[54] Tatsuya Sasaki HN, Hideaki Maeyama, Kota Mizuno. Tribology characteristics of HFO and HC refrigerants with immiscible oils - effect of refrigerant with unsaturated bond. International compressor engineering conference purdue university, Indiana, USA, 12-15 july, 2010, Paper 1946.

[55] Akram MW, Polychronopoulou K, Seeton C, Polycarpou AA. Tribological performance of environmentally friendly refrigerant HFO-1234yf under starved lubricated conditions. Wear 2013;304:191–201.

[56] Akram MW, Polychronopoulou K, Polycarpou AA. Tribological performance comparing different refrigerant–lubricant systems: the case of environmentally friendly HFO-1234yf refrigerant. Tribol Int 2014;78:176–86.

[57] Nunez EE, Polychronopoulou K, Polycarpou AA. Lubricity effect of carbon dioxide used as an environmentally friendly refrigerant in air-conditioning and refrigeration compressors. Wear 2010;270:46–56.

[58] Cannaday M, Polycarpou A. Advantages of CO_2 compared to R410a refrigerant of tribologically tested Aluminum 390-T6 surfaces. Tribol Lett 2006;21:185–92.